Structural styles of Albian rafts in the Espírito Santo Basin (SE Brazil): Evidence for late raft compartmentalisation on a 'passive' continental margin

Aldina Piedade[1], Tiago. M. Alves[1]

[1]3D Seismic Lab. School of Earth and Ocean Sciences, Cardiff University, Main Building, Park Place, Cardiff, CF10 3AT, United Kingdom

E-mail address: PiedadeAM@cardiff.ac.uk

Abstract

In recent years, hydrocarbon exploration offshore SE Brazil has been focused on Early Cretaceous units that were deformed due to Albian-Cenomanian gravity gliding above Aptian salt. A three-dimensional (3D) seismic volume from the Espírito Santo Basin, SE Brazil is here used to: a) test the parameters considered to control raft tectonics on a margin tectonically reactivated in the Cenozoic, and b) investigate the impact of prolonged halokinesis on raft deformation. Offshore Espírito Santo, the combined effects of halokinesis and multiple (Andean) tectonic phases are expressed by local collapse, fault reactivation and late segmentation of Albian rafts. As a result of this deformation we observe four main raft geometries: a) rolled-over rafts, b) tabular rafts, c) collapsed rafts, and d) folded and tilted rafts on the flanks of salt rollers. This work shows that salt rollers formed buttresses to moving Albian-Cenomanian rafts, with withdrawal of salt from underneath some of the rafts leading to their collapse and welding onto pre-salt strata. This process occurred in the studied part of the Espírito Santo Basin with minimum control of post-raft overburden thickness on raft compartmentalisation. Salt withdrawal from underneath the rafts is an important phenomenon as it enhanced connectivity between pre-salt and post-salt units, potentially promoting the migration of hydrocarbons from syn-rift source units into post-salt reservoirs.

Keywords: South Atlantic, SE Brazil, raft tectonics, compartmentalisation, halokinesis, overburden thickness.

1. Introduction

Raft tectonics comprises one of the most extreme deformation styles on salt-influenced continental margins (Duval et al., 1992; Gaullier et al., 1993; Mauduit et al., 1997; Penge et al., 1999; Alves, 2012; Pilcher et al., 2014). It is characterised by downslope translation of large blocks of strata above a ductile detachment layer (Gaullier et al., 1993). A key characteristic of raft tectonics is that thin-skinned stretching in overburden strata reaches beta (β) values of 2-3, with associated gravitational gliding contributing to the fragmentation of post-salt units (Duval et al., 1992; Gaullier et al., 1993; Mauduit et al., 1997; Vendeville, 2005). The majority of published work suggests this fragmentation results from the interaction between gliding blocks (rafts), faulting and a thickening overburden. Based largely on the interpretation of regional 2D seismic data and the analysis of physical models, published results consider the thickness of the post-raft overburden and the slope gradient as the main controlling parameters on the degree and style of raft segmentation and downslope movement (Brun and Mauduit, 2009; Duval et al., 1992; Gaullier et al., 1993; Mauduit et al., 1997; Vendeville, 2005). According to these authors, differences in post-raft overburden thickness can maintain downslope gliding of rafts even if slope gradient is close to zero, as long as an efficient basal décollement is present at depth. The proposed models essentially suggest that increasing rates of syn-kinematic sedimentation increase downslope displacement of rafts and make listric normal faulting more likely (Mauduit et al., 1997). However, the role of salt thickness and tectonic reactivation in raft evolution is still poorly understood in basins such as the Espírito Santo Basin, in which significant tectonic and igneous events are known to have controlled its structural evolution (e.g. Fiduk et al., 2004). In fact, distinct tectonic episodes controlled the Late Cretaceous-Lower Cenozoic evolution of the basin, inducing local shortening, diapir growth and fault reactivation (Fiduk et al., 2004; Baudon and Cartwright, 2008; Alves, 2012).

This work is based on 3D TWT (two-way time) seismic data from Espírito Santo Basin, offshore SE Brazil, to describe and discuss the effect of tectonic reactivation and halokinesis on the structure of Albian rafts and overlying strata. It focuses on a region of offshore SE Brazil where a direct relationship between post-raft overburden thickness and raft internal deformation is not observed, and concludes on the factors that may have controlled raft evolution in the Espírito Santo Basin (Figs. 1a to 1c). Importantly, the study area records multiple episodes of tectonic reactivation related to the Andean tectonic phases and Paleogene emplacement of the Abrolhos Volcanic Plateau (Fiduk et al., 2004) (Fig. 1a). The first of these episodes, the Late Cretaceous Peruvian phase (Scheuber et al., 1994), had a deep control on fault reactivation and local erosion in the study area. The main advantage of this work, when compared with most published data, is that it uses a high-quality 3D seismic data volume to describe in great detail the fault families associated with salt structures and adjacent rafts. In such a context, we will map and describe main faults and types of rafts in a sedimentary basin known for its hydrocarbon potential.

The paper starts with a description of the data and methods used. It is followed by a section introducing the geological setting of the Espírito Santo Basin. The results section describes the main raft geometries, quantifies overburden thickness, and documents the main fault families observed in the study area. It also relates the styles of halokinesis imaged on seismic data with the styles of deformation observed within the rafts. We conclude the paper by answering important questions related to raft evolution, including:

a) Is the thickness of post-raft overburden the key control on raft deformation offshore Espírito Santo?

b) Are growing salt structures capable of imposing renewed compartmentalisation in otherwise welded (and stable) rafts?

c) What is the importance of halokinesis to hydrocarbon migration and structure charging of Albian rafts in the study area of the Espírito Santo Basin?

2. Data and methods

A high-quality 3D TWT seismic volume from CGG was used in this paper to interpret the structural evolution of Albian-Cenomanian rafts in the Espírito Santo Basin, SE Brazil. The interpreted 3D seismic volume covers 2400 km^2 of the continental slope area immediately south of Abrolhos Plateau, in Block BES-100 (Fig. 1a). The seismic volume was acquired using a 6 x 5700-6000 m array of streamers. It has a bin spacing of 12.5m x 25 m and is zero-phased migrated. The seismic volume uses the European SEG standard for polarity, in which the a change of acoustic impedance from low to high has positive amplitude and is visualised on-screen as a red seismic reflection. Data were vertically sampled every 2 ms. Data processing included resampling, spherical divergence corrections and zero-phase conversions undertaken prior to stacking (Fiduk et al., 2004; Alves, 2012).

Four N-trending rafts were investigated to constrain their spatial distribution and deformation (Figs. 1b, 1c and 2). The top and base of the interpreted rafts coincide with a reflection of strong amplitude that was mapped every two lines (25 m). Detailed structural maps were generated to highlight the rafts' external and internal structure, and the orientation and distribution of their faults. In detail, prominent stratigraphic unconformities were mapped across the entire seismic volume to compute: (i) isochron maps for post-raft overburden units, and (ii) Root-Mean Square (RMS) amplitude maps, which are useful to highlight faults and chasms inside and between the interpreted rafts. RMS amplitude maps average the squared amplitudes of seismic reflections mapped within a pre-defined interval (Brown, 2004).

Post-raft overburden thickness was measured every 20 inlines and crosslines (i.e. every 250 m). Raft thickness, length and width were also measured to document changes in rafts geometry. Seismic stratigraphic interpretations were based on França et al. (2007) and Alves (2012). In our calculations we used velocity data from the DSDP Site 516 (located on the Abyssal Plain to the southeast of the study area), which estimated V_p velocity varying from 1700 m/s TWT for Late Cenozoic strata, to 2000 m/s for Paleogene and Late Cretaceous strata and 3500 m/s for the interpreted rafts (Barker et al., 1993). A seismic velocity of 1560 m/s TWT was used for the water column (Gamboa et al., 2012) (Figs. 2 and 3a).

3. Geological framework of the Espírito Santo Basin

3.1 Tectono-stratigraphic evolution

The Espírito Santo Basin comprises a series of Late Jurassic-Cretaceous rift basins, trending N-S to NNE-SSW, located between the Vitória-Trindade Chain and Abrolhos Plateau (Fig. 1a). Its tectonic evolution records four distinct stages: rift onset, syn-rift, transitional and drift (Alves, 2012; Chang et al., 1992; Fiduk et al., 2004; Gamboa et al., 2012). The initial rift-onset stage occurred during the Late Jurassic to earliest Cretaceous and chiefly comprises continental deposits (Figs. 3a and 3b). The syn-rift stage, dated from the late Berriasian/Valanginian to the early Aptian, is marked by significant tectonic activity that led to the formation of rift basins (Demercian et al., 1993; França et al., 2007; Gamboa et al., 2011; Mohriak, 2005; Ojeda, 1982). During this time, lacustrine sediments accumulated in a series of fault-controlled basins before carbonate deposition commenced at the start of the Aptian.

The transitional stage occurred between the Aptian and the early Albian, and records widespread tectonic quiescence with the cessation of basement fault activity (Gamboa et al., 2011). Thermally, the basin records a sudden increase in heat flow accompanying continental breakup in its more distal parts, whereas proximal regions of the margins should have recorded a relative cooling (Lentini et al., 2010). In addition, thick salt in parts of the basin was potentially able to cool the basin relatively to regions with no salt, keeping some of the pre-salt source rocks in the oil and gas windows. The effect of thick accumulations of salt is even more marked when considering discrete episodes of rifting offshore SE Brazil, each one capable of recording increases in local heat flow to the margin (Lentini et al., 2010). Stratigraphically, the transitional stage marks a shift from continental syn-rift strata to marine drift units. These units mark the first marine incursion into the central graben of the southeast Brazilian rift basins (e.g. Dias, 2005). The transitional stage in SE Brazil records the deposition of >3000 m of evaporites, mainly halite and anhydrite, resulting from extreme marine evaporation in arid climatic conditions (França et al., 2007; Mohriak, 2003; Mohriak et al., 2008).

The drift stage reflects the onset and the spreading of ocean crust between the South American and African tectonic plates and is dominated by open marine deposition. The deposition of marine shales, turbidite sands and marked episodes of mass-wasting define this stage in the Espírito Santo Basin (Fiduk et al., 2004). The drift stage can be sub-divided into a transgressive early-drift megasequence (Albian-Early Eocene) and a regressive late-drift Megasequence, which together span from Eocene to Holocene (Ojeda, 1982). In the Espírito Santo Basin, the drift stage is dominated by continental-slope embankment, incision of submarine channel systems, and widespread slope mass-wasting, with salt tectonics playing a significant role in post-evaporitic sequence deformation. Post-salt deformation in the Espírito Santo Basin has been driven by a combination of gravity gliding and gravity spreading (Fiduk, et al., 2004). Salt structures and associated overburden units can be divided into three structural domains: a) proximal extensional, b) mid-slope translational, and c) distal compressional (Fig. 3b). The extensional domain is located in proximal, upper slope areas and is characterised by salt rollers, salt walls, normal faults, turtle anticlines and rafts (Fiduk et al., 2004; Gamboa et al., 2011; Mohriak et al., 2008; Omosanya and Alves, 2013). The transitional, mid-slope domain is dominated by salt diapirs, whereas the compressional domain is developed on the distal parts of the slope and is dominated by allochthonous salt canopies and tongues that deform the seafloor (Fiduk et al., 2004) (Fig. 3b).

3.2 Andean tectonic phases and their effect on SE Brazil

The study area was affected by several tectonic events (França et al., 2007), some of which can be correlated to deformation episodes in the Central Andes (Fiduk et al., 2004; Gamboa et al., 2011; Mohriak et al., 2008; Omosanya and Alves, 2013). These deformation episodes are expressed in the Espírito Santo Basin by stratigraphic unconformities of regional expression (França et al., 2007) as shown in detail in Fig. 3a. The direction of shortening was roughly orientated E-W following the trend of the Andean Ranges, and acted together with gravitational tectonics to form complex structures at post-salt level. At the scale of the South American Plate, the Andean Orogeny was triggered in the Late Albian, during the Mochica phase (Mégard, 1984; Mégard et al., 1984), leading the formation of the Pre-Urucutuca unconformity (Horizon 3) in the study area (Fig. 3a). The following tectonic event, the Peruvian phase (80-90 Ma; Scheuber et al., 1994) resulted in the deposition of extensive turbidite-filled submarine channels, which are particularly prevalent in the study area (Fig. 3a).

A major reconfiguration of oceanic plates occurred at 49 Ma in the SE Pacific, during the Eocene Incaic phase (Isacks, 1988; Mégard, 1984) (Fig. 3a). The last Andean compressive events are divided into three discrete phases: the Quechua 1, 2 and 3 (Mckee and Noble, 1982; Mégard et al., 1984), as shown in Figure 3a. The Quechua 1 phase occurred between ~20 and 12.5 Ma (Early to Middle Miocene; Mégard, 1984), whereas the Quechua 2 phase occurred between 9.5-8.5 Ma (Pliocene) and was marked by strike-slip movements (Fig. 3a). Broadly east-west orientated shortening occurred during Quechua 3 (at ~6 Ma), which contrasts with the N-S shortening recorded at present in the eastern part of South America (Lima, 2003).

4. Controls on raft movement and segmentation

Raft tectonics is the most significant style of deformation accompanying thin-skinned extension on continental margins. Raft tectonics can generate regions in the sedimentary sequence where the overburden stretches by two or three times its original length (Duval et al., 1992; Gaullier et al., 1993; Mauduit et al., 1997). Where fault blocks at the base of stretched overburden units are disconnected, they are termed rafts. If they are still partly in contact, they are termed pre-rafts (Duval et al., 1992).

Most published studies used experimental or numerical models to understand the mechanisms of raft tectonics (Duval et al., 1992; Gaullier et al., 1993; Mauduit et al., 1997). These models were often supported by 2D seismic data, and they were based on various assumptions concerning the physical processes involved in rafting. Such seismic data were crucial to understand the mechanical behavior of raft systems and test the applicability of physical and numerical models (Brun and Fort, 2011).

One of the key parameters mentioned in published models as capable of controlling raft displacement is overburden thickness (Mauduit et al., 1997). In their physical analogue models, Mauduit et al. (1997) tested how the rafting structures are controlled by overburden sedimentation. The experiment resulted in the formation of a wide deformation zone in the lab, with tilted blocks delimited by extensional normal faults and rafts (Figs. 2 and 4). The first structures to develop are symmetric grabens and, as sedimentation rate increases, the number of rafts or blocks increase proportionally (Fig. 4). The models of Mauduit et al. (1997) indicate that an increase of the sedimentation rate enhances the displacement rate of rafts as a response to increasing vertical loading. Vendeville (2005) later showed that regional sediment deposition can trigger gravity spreading, even without an oceanward dipping basal slope. As a key example, rafts in the Gulf of Mexico record pure spreading driven by sedimentary loading. This setting requires a thick sedimentary overburden, high sediment density and low frictional angles of the sediments (Brun and Fort, 2011; Rowan et al., 2012). It will also imply the creation of large amounts of lateral space into which overburden units can accumulate during stretching, as recorded in the Kwanza Basin (Angola) by Duval et al. (1992). Here, two different types of gravity related movements have been identified; gravity gliding and gravity spreading.

Salt as a viscous evaporitic layer has been described as an important factor not only in raft formation, but also in raft gliding and subsequent deformation (Brun and Mauduit, 2009, Vendeville, 2005,). Salt acts as a lubricant layer and forms rollers, pillows and diapirs adjacent to individual rafts (Alves, 2012; Brun and Mauduit, 2009; Gaullier et al., 1993). Brun and Mauduit (2009) performed laboratory experiments to study the development of growth faults during rafting. They suggested that the concave shape of rollover faults is not the only valid argument for the generation of large-scale listric faults in areas of raft tectonics. Instead, their concave shape results from the connection between a steeply dipping normal fault and a flat-lying or gently dipping décollement, a geometry prone to cause important tectonic reactivation in adjacent rafts due to the mechanical instability of rollover faults (Brun and Mauduit, 2008). In other words, changes in the dip of roller faults at depth results in the transfer of horizontal displacement towards the surface through the rolling over of strata in the rafts, and in post-raft overburden strata every time roller fault sole out into the detachment salt layer and significant lateral movement is recorded in rafts. In support of this, Alves (2012) documented significant Late Cretaceous-Early Cenozoic reactivation in raft-related faults in the Espírito Santo Basin, a phenomenon triggered by regional (Andean) tectonics and related slope oversteepening.

This paper develops the ideas of Alves (2012), recognizing that the thickness of post-raft overburden units does not vary significantly in the study area, a character suggesting that the salt thickness and the evolution of salt rollers are the main controlling factor in their compartmentalization and ramping up on the flanks of growing salt rollers. For that reason, we name this latter stage of thin-skinned deformation ‘late rafting’, as it occurred in the late Cretaceous after the main stage of raft movement in the Espírito Santo Basin.

5. Seismic stratigraphy and structural features of the Espírito Santo Basin

The seismic stratigraphy of the Espírito Santo Basin follows França et al. (2007), Alves and Cartwright (2009) and Alves (2012). Figures 2 and 3a show seismic sections illustrating the entire seismic sequence and the horizons interpreted in this work: a) base raft (Horizon 3a), b) top raft (Horizon 3), c) base Santonian (Horizon 4) and d) the seafloor. In the next few paragraphs the seismic imaging and a lithological description of the complete sedimentary sequence are described.

5.1 K20 to K40 sequence (Earliest Cretaceous to Early/Mid Aptian)

The K20-K40 sequences comprise sub-salt, syn-rift and early post-rift strata. The lower boundary of K20 is marked by a moderate-amplitude, locally diffractive reflection marking the top of crystalline basement rocks. The contact between K20 and K30 is irregular, and the imaged sequences comprise moderate to high amplitude, low frequency reflections. K40 has a higher amplitude and is more continuous than K20 and K30 (França, et al., 2007). The boundaries between K20, K30 and K40 are difficult to distinguish on the interpreted seismic volume, partly because the sequences comprise moderate to high amplitude, low frequency reflections (Fig. 6).

K20 comprises the oldest unit in the study area (Valanginian), deposited at the base of the Nativo Group (Cricaré Formation). Heterolithic conglomerates and coarse sandstones observed in proximal regions of Espírito Santo grade into fine-grained mudstones in more distal areas (França et al., 2007). The K30 sequence comprises volcanic and volcaniclastic rocks intercalated with sandstones and conglomerates (Jaguaré Member), which change into shales, marls and carbonate units in more distal regions (França et al., 2007). The basal post-rift Sequence K40 comprises conglomerates and sandstones that grade into fine sandstones and shales deposited in lacustrine and sabkha environments (Membro Mucurí) (Figs. 3a and 6).

5.2 K50 sequence (Aptian)

The K50 sequence represents the main salt interval in the Espírito Santo Basin. This unit is particularly well imaged forming the core of salt pillows and diapirs, where it is characterized by chaotic, low amplitude reflections (Fig. 6). Its lower boundary consists of an irregular, moderate to high amplitude reflection, below which high amplitude strata are observed. Its upper boundary coincides with the first continuous strata above the low amplitude salt structures. In the study area, the K50 sequence is only preserved within triangular salt anticlines (rollers) formed between rafts (Fig. 6).

K50 was deposited in a series of confined basins in conditions of high evaporation. Carbonate and anhydrite intervals predominate in shallow marginal areas of Espírito Santo, whereas halite is more abundant in the central and distal parts of the basin (França et al., 2007).

5.3 K62 to K70 sequences (Albian)

The K62 to K70 sequences comprise a package of high-amplitude internal reflections overlying the K50 and the basal K20 to K40 sequences. The lower boundary of K62-K70 is marked by Horizon 2, whereas the top (i.e. Horizon 3) comprises an angular unconformity in the study area (França et al., 2007).

K62-K70 is up to 600 ms two-way travel time thick and comprises marine strata, mainly sands, silt, shales and oolitic limestones and marls, which are partly time equivalent to Unit 7 at DSDP Site 356 (Kumar et al., 1977) and to the onshore Regência Formation (Bruhn and Walker, 1997; Fiduk et al., 2004; França et al., 2007) (Fig. 3a). The top of K62-K70 is an angular unconformity in the proximal regions of the Espírito Santo Basin, changing into a paraconformity in more distal regions (França et al., 2007).

The two-way time structure of the top raft Horizon 3 is shown in Figure 7a. The map reveals the presence of six (6) rafts in the study area, which are separated by local chasms (Fig. 7a). These isolated depocentres were filled by post-Albian strata as explained in the following section (Figs. 3a and 8).

5.4 K82 to K88 sequences (Late Albian to Santonian)

The K82 to K88 sequences comprise continuous, low-amplitude reflections deposited above the Albian-Aptian rafts and associated salt structures. The lower boundary of K82-K88 is sharp and marked by growth onto major listric faults above Horizons 2 and 3. The upper boundary of Late Albian-Santonian strata is an irregular high-amplitude reflection representing an erosional unconformity of Santonian age (Horizon 4) (França et al., 2007).

The K82-K88 sequences comprise shales and turbidite sands (França et al., 2007), belonging to the lower Urucutuca Formation (Fig. 3b). Locally, the lower boundary of K82 contains carbonate breccias derived from eroded Albian carbonate platforms.

In Figs. 7b and 7c are highlighted the two-way time structure and thickness of Late Albian-Santonian sequence. Deposits of this latter age fill local inter-raft basins and cover older rafts to a maximum thickness of 3.5 s (~2700 m) over raft 4 (Fig. 8). Isochron maps show a minimum thickness over structural highs (i.e., rafts) and structures reactivated at the end of the Cretaceous (Figs.7b and 7c). Main sub-basins and associated salt rollers strike N-S to NNE-SSW (Figs. 7b and 7c).

5.5 K90-K130 sequence (Late Santonian to Maastrichtian)

A major unconformity related to the incision of a Late Santonian to Maastrichtian channel system is observed above low-amplitude strata in K82-K88 (Golfinho Field, Vieira et al., 2007). This boundary (Horizon 4, Fig. 3a) is overlaid by high-amplitude seismic reflections. Growth of strata into listric, salt-detached faults is observed below the unconformity (Fig. 9). A regional unconformity of Late Maastrichtian age marks the upper boundary of K90-K130.

K90-K130 comprises the middle part of the Urucutuca Formation (Fiduk et al., 2004; França et al., 2007). The main lithologies in the sequence are turbidites and shales, changing into marly successions towards more distal parts of the Espírito Santo Basin (França et al., 2007).

The two-way time isopach of K90-K130 is shown in Fig. 7c. The figure highlights the complex set of faults that developed in this sequence, partly in response to basin reactivation at the end of the Cretaceous. Reactivated structures at K90-K130 level are shown with thickness minima in the study area, a character further investigated in Section 6 (Figs. 7c and 9).

5.6 E10-E30 sequence (Paleocene to Early Eocene)

The E10-E30 sequence comprises high-amplitude reflections affected by closely-spaced normal faults. Its lower boundary coincides with the Maastrichtian unconformity (Fig. 3a), whereas the upper boundary is marked by Horizon 6, a regional unconformity above which moderately faulted reflections are observed. This unconformity has been interpreted to result from tectonic uplift of the basin-shoulder during the early Cenozoic (França et al., 2007). A key characteristic of this interval is the high degree of faulting observed to extend from Upper Cretaceous strata (Fig. 10).

5.7 E40 to N10 sequences (Eocene to Early Miocene)

The E40 to N10 sequences are composed of east-dipping clinoforms deformed by closely-spaced normal faults (Figs. 3a and 9). The age of E40-N10 ranges from the Eocene to the Early Miocene, i.e. it comprises equivalent strata to the upper part of the Urucutuca Formation (França et al., 2007). The E40-N10 sequences are composed of turbidite sands intercalated with volcaniclastic deposits

(França et al., 2007). There is evidence on seismic data that syn-sedimentary fault activity continued at this level. (Figs. 9 and 11)

5.8 N20 to N60 (Early Miocene to Holocene)

The N20-N60 sequences comprise chaotic to continuous reflections. The sequences are, in places, eroded by submarine channels and comprise sandstones (Rio Doce Formation), calcarenites (Caravelas member) and turbidite sands and marls (Urucutuca Formation). Mass-transport complexes and channel-fill deposits are abundant throughout the basin after the Early Miocene (França et al., 2007) (Fig. 3a).

The mid-Miocene TWT structure in Figure 10 shows the complex faulting observed at this level, and the formation of a gentle slope dipping towards the east.

6. Results

6.1 Evidence for tectonic reactivation and late halokinesis

The Andean tectonic phases were key events controlling the structural evolution of the Espírito Santo Basin (Lima, 2003). Tectonic reactivation was chiefly recorded at the end of the Cretaceous and in the Eocene, as revealed on seismic data. Figure 7 shows a series of isochron maps between the Maastrichtian and Santonian unconformities i.e., between the stratigraphic unconformities that mark Late Cretaceous and Eocene tectonic episodes in the Espírito Santo Basin (Alves, 2012). In these maps is important to highlight the thickness variations recorded at Santonian-top Maastrichtian and Maastrichtian-Eocene levels. Areas recording reactivation and local erosion present the lower thickness values in Figure 7. On seismic data, tectonic reactivation on seismic data is marked by low-amplitude folding and reactivation of extensional structures (Figs. 2 and 5).

Erosion of Horizons 5 and 6 accompanied Late Cretaceous and continued during Eocene tectonism, and resulted in the deposition of less than 400 ms TWT between the two mapped unconformities (Fig. 5).

Figure 8 illustrates one of the regions on the Espírito Santo continental slope where tectonic reactivation is more pronounced. Reactivated faults occur in the imaged seismic line between rafts 1 and 2, towards the upper part of the continental slope. In other regions, pop-up structures intersect Late Cretaceous and early Cenozoic strata (Figs. 2 and 5).

In summary, Late Cretaceous tectonic reactivation on the Espírito Santo continental slope area is marked by: a) localised inversion of raft-bounding normal faults, forming local pup-up structures b) shortening of Meso-Cenozoic strata to form local pop-up structures (Fig. 2).

6.2 Rafts geometry and thickness variations in the post-raft overburden

At present, Aptian salt forms isolated accumulations, some of which are observed beneath the interpreted rafts in the form of rollers. Above the Aptian salt are observed symmetric and asymmetric rafts with distinct structural styles and inferred evolutions (Figs. 5 and 6).

A structural map of Horizon 3 (top rafts) illustrates the plan-view geometry of rafts 1 to 6 (Fig. 7a). In the northwest part of the study area, the rafts are intensely faulted. In east-west profiles, i.e. perpendicular to the strike of rafts, raft 1 is irregular and discontinuous, showing important segmentation (see Section 7 and Fig. 7a). In the map in Fig. 7a, this raft is at least 36 km long. For raft 2, two-way time (TWT) raft thickness ranges from 34 ms to 815 ms along the north-south profile in Fig. 11. This corresponds to a thickness of 45 m to 1107 m, using velocity data from Barker et al. (1983) (Fig. 3a).

In contrast to raft 1, the north-south profile in Fig. 11 shows raft 2 to be continuous with a well-defined branch in its northeast portion. The gap between the main body of the raft 2 and this latter branch is occupied by a chasm with a small salt roller (Fig. 6). The TWT thickness of raft 2 varies between 52 ms and 991 ms, i.e. between 72 m and 1340 m. Rafts 3 and 4 are geometrically similar without any visible branches developed along their long axes (Figs. 1b and 7a). Raft 4 comprises a north-trending raft with a tabular shape showing distinct degrees of bucking and faulting at Cretaceous level (Figs. 1c and 6)

Rafts 5 and 6 are the structures less visible on seismic data, with their base outside the available seismic data in most of the study area (Fig. 1c). Their tops are irregular, with several segments visible on structural data (Fig. 7a). Aptian salt is present as isolated accumulations (rollers) beneath of rafts 1 to 6.

Thickness plots were calculated from seismic data (Fig. 12). The plots are separated into two main packages comprising post-raft sediments: (i) top rafts (Albian to Early Cretaceous) to base Santonian (Late Cretaceous) and (ii) top rafts (Albian to Early Cretaceous) to seabed (Figs. 3a, 5 and 6). Over the northern part of raft 1, overburden thickness is 700 ms (875 m) from top raft to the base Santonian (K82 to K88 sequences); and 1280 ms (~1600 m) for the Santonian to the seafloor (K90 to N60 sequences) (Fig. 12). Trend curves for overburden thickness are similar for the two intervals considered: top raft to base Santonian and base Santonian to seafloor, and when plotting the curves for the total post-raft overburden (Fig. 12).

Overburden strata draping rafts 2 and 3 show a similar thickness trend to equivalent strata above raft 1, recording ~1250 ms (1562 m) and 2600 ms (2860 m) for the top raft to base Santonian, and base Santonian to seafloor intervals (Fig. 6). Strikingly, rafts 4 and 5 show marked thickness variations in north-south profiles, but with the thicker overburden strata occurring to the north and central parts of the rafts, where structural compartmentalisation is greater (Fig. 12). Raft 6 shows larger thickness in its central part (Fig. 12). In essence, the thickness of post-raft overburden increases towards the south when considering the sequences between Horizon 4 and 5, and decreases for the Santonian-Seafloor sequence (Fig. 12).

6.3 Deformation styles and fault families

Figure 7c shows an isochron map between Horizons 4 and 5 (Santonian to top Maastrichtian). In addition, the seismic profiles in Figures 5, 6 and 8 highlight the main fault families developed above the Aptian salt and in Albian rafts. Figure 7c is complemented by the TWT structural maps in Figure 10. The maps show the complex sets of faults affecting post-salt overburden units near the base of the Santonian and above. The seismic profiles in Figure 8 show that overburden faults propagated vertically until they reached horizon 4 (base Santonian) and overlying strata. Fault families in rafts 1 to 6 include: a) roller, b) rollover, c) keystone; d) reactivated, and f) concentric faults. A schematic map of these types of faults is shown in Figure 13.

6.3.1. Roller Faults

Roller faults accommodated bulk downslope displacement in rafts. Roller faults dip both oceanwards (east) and landwards (west), offsetting strata in rafts 1 to 4 and overlying strata above them (Figs. 5, 6 and 8). Roller faults sole out into the Aptian salt. Triangular salt rollers are observed in the footwalls of roller faults (Fig. 14). Some of the roller faults propagated upward into lower Cenozoic strata, tipping out at the base of a mass-transport deposit that contains large remnant blocks (Alves, 2012).

6.3.2 Rollover Faults

Rollover faults comprise closely-spaced antithetic and synthetic faults generated on top of monoclinal rollovers and turtle anticlines, themselves formed due to movement on adjacent roller faults. Together with keystone faults, rollover faults accommodate some of the bending strain related to the downslope displacement of collapse of underlying rafts (Fig. 15). They are formed due to progressive bending of rollover structures above the Albian rafts (Fig. 5, 6 and 8).

6.3.3 Keystone faults

Keystone faults are pairs of conjugate normal faults that dip in the opposite direction to, and accommodate displacement occurring on rollers faults (Figs. 5 and 6). Keystone faults can also manifest as planar growth faults rooted into the crests of triangular salt rollers. Throws on keystone faults are small in the regions where they intersect collapsed salt rollers (Alves, 2012) (Fig. 16).

6.3.4 Reactivated faults

Reactivated faults comprise fault sets initially formed by the arching of overburden units above the Albian rafts. They were later reactivated in late Cretaceous anticlines, as shown in Fig. 8. The geometry of reactivated roller faults resemble that of crestal (or keystone) faults, but they form anticlinal structures towards their top (Figs. 9d and 13). They are interpreted as rollover, keystone and crestal faults that were reverse-reactivated.

6.2.5 Concentric faults

Concentric faults are observed above the depocentres formed by raft tectonics (Alves, 2012) (Fig. 9c and 9b). They are developed on the margins of extensional sub-basins, dying out downwards the main Cretaceous depocentres, accommodating local strain at the tips of the oval-shaped sub-basins formed on the hanging-wall blocks of roller faults.

7. Structural styles documenting raft deformation over Aptian salt structures

7.1. Rolling-over and internal strata growth

Rolled-over rafts are those showing important growth of strata adjacently to salt rollers and roller faults (Fig. 10). These rafts are not cross-cut by major faults, and are mostly bounded landwards and oceanwards by large roller faults. Rolled-over rafts formed during Cretaceous gravitational collapse of the margin, but with most of extension concentrated on the larger roller faults. Turtle-back structures are not developed above these rafts (Figs. 5 and 8).

The raft imaged in Figure 14 show important growth of strata in the areas where salt was withdrawn from the base of the raft towards adjacent salt pillows. It is also noted the increasing angle of basal strata in the raft as the rolling-over of the raft continues in time (Fig. 8).

7.2 'Passive' fragmentation in the form of tabular rafts

Tabular rafts are structures displaced over salt without significant control of roller faults on the growth of strata inside the rafts (Figs. 8 and 15). Instead, these rafts are interpreted to have evolved with large salt rollers separating them from adjacent rafts, and hindering any rolling over of strata on their flanks (Figs. 8 and 15). Faults are scarce in their interior and, when present, show predominant normal offsets resulting from salt withdrawal at flanks of the rafts. Turtle anticlines can form in younger overburden units in response to folding of latest Cretaceous-early Tertiary strata (Fig. 11).

Figure 15 shows tabular raft 2 in the study area of Espírito Santo. Tabular rafts show no significant growth of strata in their interior, suggesting they were 'passively' translated and fragmented on the continental slope. In the study area, most of the tabular rafts seem to be partly welded on pre-salt successions and are bounded my small to moderate size salt rollers that did not deformed their flanks (Fig. 15).

7.3 Collapse and folding of rafts' flanks due to salt withdrawal

Collapsed blocks are observed in flanking strata to sub-tabular rafts, always in association with withdrawal of salt from evolving salt rollers (Fig. 16). Resulting fault styles include normal faults showing no growth at the level of the Albian rafts, but showing growth and erosional truncation at Late Cretaceous level (Fig. 16). This character suggests the faults post-date the deposition of Albian-Cenomanian strata drapping the interpreted rafts. As a result of the withdrawal of salt from salt rollers, most of these collapsed blocks are, at present, welded onto pre-salt successions (Fig. 16).

Rafts are usually folded in the immediate footwall of the larger roller faults (Fig. 16). They reflect later growth of roller faults and associated growth of salt rollers on the flanks of relatively stable rafts. Roller faults show predominant normal offsets and, in some parts of the study area, were reactivated to form pop-up structures expressed in Upper Cretaceous strata.

Figure 16 depicts collapse structures in raft 2. Here, we interpret the withdrawal of salt from underneath the raft, and subsequent growth of the salt pillow to the west, resulted in the collapse of the flank of the imaged rafts. This structural style is more obvious to the north of the study area, where rafts 1 to 6 are close together and segmented in smaller rafts. Local collapse structures accompany the tilting and fragmentation of rafts on the flanks of salt rollers that grew, or where shortened, during the Late Cretaceous and Cenozoic.

7.4 Tilting and fragmentation of rafts on the flanks of growing salt rollers

The most striking example of late reactivation in rafts comes from the array of faults and rafts formed and tilted on the flanks of growing salt rollers. An example of one of such structures is shown in Fig. 12, in which the oceanwards half of raft 2 is fragmented, collapsed and tilted on the flank of the salt roller separating raft 2 into two parts. Normal faults related to the collapse of rafts over withdrawn Aptian salt are observed in Figs. 6 and 16). Faults show predominant normal offsets resulting from extension and salt withdrawal, but do not extend up into Paleogene strata i.e., they were chiefly generated by short-lived collapse of rafts during the Late Cretaceous. As a result of collapse, complex sets of conjugate normal faults are often observed in Upper Cretaceous rollovers, as structures formed to accommodate the collapse of underlying rafts (Fig. 16).

Figure 16 shows and example of such structural style. The imaged raft was tilted and fragmented on the flank of a growing salt roller, which shows evidence for Late Cretaceous reactivation. Part of this fragmentation results from withdrawal of salt from the base of the rafts to inflate the adjacent salt pillow, thus resulting in complex structural compartmentalisation of intra-raft strata.

8. Discussion

Fiduk et al. (2004) assumed tectonic contraction in post-salt units began early in the Albian and continued until the present day. Rafting ceased at different times depending on the initial thickness of the salt available and overburden thickness. Based on these two principles, we discuss in this section: (i) the different styles of deformation observed on the rafts and (ii) reactivation of faults as a function of salt roller growth.

8.1 Why is there a poor correlation between overburden thickness and the degree of raft deformation?

The key question posed by this work is why there is a poor correlation between overburden thickness and the degree of raft deformation in the Espírito Santo Basin? Based on the evidence of moderate, but widespread tectonic reactivation of the continental slope during the Late Cretaceous and Eocene, a plausible explanation should consider important raft movement in Espírito Santo after the Santonian. An example of late-stage raft tectonics, in which the reactivation of salt rollers is a key control on rafts' structural deformation, is provided by raft 2 (Figs. 10 to 12). Ramped-up strata on the flanks of a salt roller, with associated uplift and erosion of the Late Cretaceous Horizon 4 demonstrates a later stage of deformation in the study area (Figs. 5 and 6). We interpret this geometry as reflecting late evacuation of evaporites from upper-slope regions of the Espírito Santo Basin to the base of the continental slope. Downslope salt flow resulted in the collapse of minor salt pillows below individual rafts, in the growth of the larger salt rollers, and in the progressive welding of rafts 1 to 6 onto pre-salt units. Most of this collapse occurred in the Late Cretaceous, as shown by the collapse faults developed above Horizon 4.

The history of gravity-gliding extension of the Albian rafts and the relationship with Aptian salt layer are summarized in Figure 17. At the scale of the interpreted 3D seismic volume, we observe that syn-kinematic sediment thickness is relatively constant, a character suggesting that vertical loading imposed by overburden strata was not the key factor controlling raft movement and deformation in the study area. Instead, lateral spreading and downslope gliding of the rafts was likely controlled by the presence of intra-raft salt structures – which closely controlled the degree of downslope movement and faulting experienced by rafts 1 to 6 (Figs. 14 to 17).

Based on the interpreted data, we suggest that 'late' compartmentalisation of rafts offshore Espírito Santo is an important phenomenon, with overburden thickness playing only a minor role. In this work we demonstrate that salt rollers and the relative thickness of salt underneath individual rafts are the main factors controlling raft movement. In regions where raft movement was overprinted by the growth of salt rollers, rafts are highly segmented by reactivated faults (Figs. 5, 6, 9 and 17). In regions where smaller volumes of salt were available below the rafts and ramping-up over growing salt rollers was hindered, we suggest rafts were static throughout most of their late evolution and structural compartmentalisation was accordingly moderate.

A second question that arises when interpreting the seismic data in this paper is why are structural collapse, tilting and local deformation so prominent in raft 2? One possible answer to this question assumes that extension-related faulting was predominant in the study area, and that no major reactivation occurred in response to the Andean tectonic stages. A second potential explanation is that tectonic reactivation was significant, and that a later stage of roller growth and salt withdrawal may have occurred, even if in a predominantly extensional regime.

Locally reactivated faults and associated pop-up structures indicate that a late stage of horizontal shortening affected the study area, particularly during the latest Cretaceous and Palaeogene (e.g. Alves, 2012) (Figs. 8 and 17). These structures were previously interpreted as partly accommodating strain across the hinge of extensional rollovers. We interpreted them as reflecting a later stage of gravitational gliding in the study area, in which Late Cretaceous strata (K82-K88) were compressed against Aptian rafts (and overburden strata) due to the change from vertical subsidence, recorded on the upper part of roller faults, to sub-horizontal strain in the regions where roller faults sole into the Aptian salt (Alves, 2012).

We interpret deformation in raft 2 to result from the combination of factors described above, but the surprising result in our analysis is that the thickness of the sediments overburden is not a key factor in the onset of late raft deformation. Instead, we suggest that deformation in raft 2 resulted from a combination of factors, including slope oversteepening and resulting stresses imposed by a gravitationally unstable, downslope-moving overburden sequence against rafts 1 to 6. In this model, the evacuation of salt from beneath the rafts, and their eventual grounding, was an important process controlling the degree of deformation in Albian-Cenomanian rafts. Rafts overlying thin salt successions were quickly grounded, and faults mostly occur within Late Cretaceous-Early Cenozoic overburden strata (Figs. 5 and 6). Rafts with significant thickness of salt underneath record important collapse, with salt withdrawal contributing to the growth of adjacent salt rollers. The combined effect of salt roller growth and horizontal shortening of these same salt structures (contributing to an increase in the angle of rollers' flanks) acted together to further tilt and deform Albian-Cenomanian strata (Fig. 17). As a result, we observe in the study area styles of raft compartmentalisation distinct to those published in the literature, with the thickness of overburden units and slope oversteepening being locally replaced, as primary factors in raft compartmentalisation, by the thickness of available salt below and adjacent to fully developed rafts.

8.2 Importance of collapse features to the generation of salt welds

Salt welds are formed at the base of post-salt strata by the complete evacuation of salt from below these strata (Jackson and Cramez, 1989; Rowan et al., 1999). A consequence of welding of post-salt strata onto pre-salt units, in relationship with the timing of potential hydrocarbon generation and migration, is the establishment of fluid conduits between stratigraphic intervals that, otherwise, would be hydrodynamically separated (Rowan, 2004). A key observation from the interpreted seismic data is the generation of salt welds in regions recording collapse and tilting of strata on the flanks of salt rollers (Fig. 17). In these cases, the timing in which the salt was withdrawn from the base of the rafts, and a full weld was formed, is an important piece of information when assessing the degree and timing of connectivity between pre-salt and post-salt units. An example of these salt welds in shown in Figures 11 and 15, in which only a small part of the raft is in contact with pre-salt strata (salt weld). We postulate that most of this welding occurred relatively late in the Espírito Santo Basin, allowing the migration of fluids from pre-salt source intervals into rafts and Cretaceous reservoirs only after welds were present below individual rafts. This is an important observation, and one that confirms that palaeoreconstructions of raft movement, and fluid migration, are key to explaining discrepancies in the charging of post-salt reservoirs on continental margins dominated by gravitational collapse. The reasons for such discrepancies are highlighted in the following paragraphs.

8.3. Enhanced petroleum potential of post-salt strata due to raft grounding and salt welding

After the deposition of Aptian salt, an Albian carbonate platform was developed all over SE Brazil and later fragmented over a progressively thinner salt layer (e.g. Demercian et al., 1993). According to Mauduit et al. (1993), sediment prograding from the continental shelf may have helped this process in a first stage. In a second stage, tectonic pulses led to further oversteepening and remobilisation of the Aptian salt, resulting in enhanced halokinesis, folding and faulting of the Meso-Cenozoic successions capping the rafts (Fig. 17).

An immediate result of salt withdrawal from below the Aptian rafts is the generation of important fluid flow paths from pre-salt source units (Lagoa Feia equivalent) towards reservoir successions in and above rafts (Fig. 18). Complete withdrawal of salt from below the rafts leads to the formation of salt welds, with subsequent transmission of fluids from below the salt into post-salt successions across areas where salt thickness is below a certain threshold, or where salt is impure to allow fluid flow through it. This phenomenon has important implications to the petroleum potential of the Espírito Santo Basin; broad salt welds will favour the migration of fluids to the interior of rafts, and through the large listric faults that bound them (Figs. 17 and 18). In turn, the presence of relative thick salt below the rafts will isolate the post-salt reservoirs from pre-salt sources, with the added cooling effect of salt to the overall thermal evolution of the basin (Lentini et al., 2010).

In the study area, evidence of fluid flow through listric faults is ubiquitous in the southern part of the 3D seismic volume, where dim zones likely associated with the presence of gas are observed over raft 3 (Fig. 18). Upper Cretaceous channel-fill deposits overlie the dim zones and hint at fluid charging from pre-salt source rocks into the Golfinho Field and other associated oil and gas accumulations (Fig. 18). This setting is, nonetheless, complicated by the presence of post-Cretaceous faults that were associated with progressive halokinesis and younger tectonic phases affecting the Espírito Santo Basin. Structural and stratigraphic hydrocarbon traps subsequently formed at Late Cretaceous level could have been breached by fault families developing in Cenozoic seal units (Fig. 18). To understand the sealing capacity of such faults is paramount to assessing the petroleum potential of Late Cretaceous reservoirs.

Closer to the Andes, tectonics has been an important factor controlling the development of structural traps, and promoting fault-related paths for hydrocarbon migration from source to reservoir rocks. Examples of such control are well expressed in the Colombian Caribbean margin

(Sarmiento and Rangel, 2004; Ortiz-Karpf et al., 2015), onshore Colombia (Dengo and Covey, 1993; Mora et al., 2006), in Venezuela (Roure et al., 1997) and in multiple locations along the Argentinian Andes (e.g. Belotti et al., 1995). A similar tectonic evolution is observed in SE Brazil, where the combined effect of Andean tectonic phases and gravitational tectonics was capable of controlling trap formation and, on a larger scale, source rock maturation (e.g. Beglinger et al., 2012). The maturation history of the proximal margin of SE Brazil indicates that fault-controlled fluid migration and overburden exhumation occurred in association with the Andean tectonic phases (Mello and Maxwell, 1991). However, differences between distinct basins (and individual depocentres) are observed in relation to the degree and timing of trap formation, and thermal maturation of the basin. Assuming a homogeneous distribution of pre-salt source units, thermal maturation and fluid migration is highly dependent on the thickness of Aptian salt (Lentini et al., 2010).

In the study area of Espírito Santo, tectonic inversion is relatively moderate, but may have increased raft segmentation and overburden folding to favour (1) the reactivation of salt minibasins and detachment of overburden rocks over areas of thick evaporites; (2) forced folding of the post-Aptian overburden, particularly against grounded rafts; (3) the reactivation of slope-bounding normal faults and associated tilting of the slope area, promoting the formation of extensional and compressional forced faults over reactivated structures (Figs. 17 and 18). In addition, some of the structural traps observed at depth, particularly those related to individual rafts, might not be related uniquely to Andean tectonism. This latter aspect broadens the range of potential traps on the Espírito Santo Basin, increasing the range of drilling targets towards older Albian-Cenomanian successions capping the extensional rafts (Fig. 17).

As a result of such setting, grounding of and enhanced segmentation of rafts will favour the transmission of pre-salt fluid into the post-salt reservoirs, either by diffusion of oil through permeable strata or by directed flow through faults and fractures. Late Cretaceous–Early Cenozoic tectonics was therefore important for the relative development of traps and, in turn, for the loss of fluids through the development of faults in post-Cretaceous units. The degree of segmentation observed in rafts, and faults developed above them, denote that overburden thickness did not exclusively control raft tectonics, and Late Cretaceous-Cenozoic tectonism is proposed here to be an important control on salt withdrawal and raft segmentation well after the Albian-Cenomanian onset of halokinesis offshore Espírito Santo.

9. Conclusions

This paper shows that the most developed styles of faulting and raft compartmentalisation occur where salt was withdrawn from the base of rafts in the Late Cretaceous/Early Cenozoic. This withdrawal likely resulted from tectonic imbalance between overburden loading and slope gradient imposed by the Andean tectonic phases affecting SE Brazil. As a result, we observed the following types of structures in rafts from the Espírito Santo Basin:

a) Rolling-over and internal strata growth in rafts that were displaced in the Albian-Cenomanian;
b) Fragmentation in the form of sub-tabular rafts whenever they were 'passively' translated on the continental slope;
c) Collapse of rafts' flanks due to salt withdrawal from beneath them;
e) Tilting and fragmentation of raft on the flanks of growing salt rollers.

In the study area, rafts with significant thickness of salt underneath record important collapse, with salt withdrawal contributing to the growth of salt rollers. The combined effect of salt roller growth and horizontal shortening of these same salt structures acted together to further tilt and deform Albian-Cenomanian strata. As a result, we observe in the study area styles of raft compartmentalisation distinct to those published in the literature, with the thickness of overburden units and slope oversteepening being as primary factors in raft compartmentalisation.

A result of this setting is the relative enhancement of fluid flow through listric faults. Upper Cretaceous channel-fill deposits overlie the dim zones and hint at fluid charging from pre-salt source rocks into younger strata. This setting is complicated by the presence of post-Cretaceous faults. To understand the sealing capacity of such faults is paramount to assessing the petroleum potential of Late Cretaceous reservoirs.

It is suggested that similar settings to the one documented in this paper occur in other Atlantic-type margins subject to raft tectonics, with ramping-up of reactivated rafts contributing to a larger degree of faulting and deformation in Albian reservoirs. The data in this paper will add to future palaeoreconstructions of raft movement, and associated fluid migration from pre-salt units in SE Brazil, and will help to tackle any discrepancies in the interpretation of gravitational collapse on continental margins.

Acknowledgments

The authors acknowledge CGG permission to publish this work. Aldina Piedade thanks FCT-Portugal, PhD grant SFRH/BD/79052/2011, British Society for Geomorphology Postgraduate Conference Attendance Grant and TEPA's RAFT consortium for supporting her PhD project. The authors acknowledge Christopher Jackson, L. Moscardelli and three anonymous reviewers for their constructive comments. M&PG editor J. Craig is also acknowledged for his comments.

References

Alves, T.M., 2012. Scale-relationships and geometry of normal faults reactivated during gravitational gliding of Albian rafts (Espírito Santo Basin, SE Brazil). Earth and Planetary Science Letters, 80-86.

Alves, T.M., Cartwright, J.A., 2009. Volume balance of a submarine landslide in the Espírito Santo Basin, offshore Brazil: Quantifying seafloor erosion, sediment accumulation and depletion. Earth and Planetary Science Letters 288, 572-580.

Barker, P.F., Buffer, R.T., Gombôa, L.A., 1993. A seismic reflection study of the Rio Grande Rise. Barker, P. F., Carlson, R. L., Hohnson, D. A. (Eds.), Initial Reports of the Deep Sea Drilling Program. Government Printing Office, Washington, D. C., 953 - 976.

Baudon, C., Cartwright, J., 2008. The kinematics of reactivation of normal faults using high resolution throw mapping. Journal of Structural Geology 30, 1072-1084.

Beglinger, S.E., van Wees, J.-D., Cloething, S., Doust, H., 2012. Tectonic subsidence history and source-rock maturation in the campos Basin, Brazil. Petroleum Geoscience 18, 153-172.

Belotti, H.J., Saccavino, L.L., Schachner, G.A., 1995. Structural Styles and Petroleum Occurrence in the Sub-Andean Fold and Thrust Belt of Northern Argentina. AAPG Memoir 62, 545–555.

Brown, A.R., 2004. Interpretation of three-dimensional seismic data, Sixth ed. American Association of Petroleum Geologists, Tulsa.

Bruhn, C.H.L., Walker, R.G., 1997. Internal architecture and sedimentary evolution of coarse-grained, turbidite channel-levee complexes, Early Eocene Regência Canyon, Espírito Santo Basin, Brazil. Sedimentology 44, 17-46.

Brun, J.-P., Fort, X., 2011. Salt tectonics at passive margins: Geology versus models. Marine and Petroleum Geology 28, 1123-1145.

Brun, J.-P., Mauduit, T.P.O., 2008. Rollovers in salt tectonics: The inadequacy of the listric fault model. Tectonophysics 457, 1-11.

Brun, J.-P., Mauduit, T.P.O., 2009. Salt rollers: Structure and kinematics from analogue modelling. Marine and Petroleum Geology 26, 249-258.

Chang, H.K., Kowsmann, R. O., Figueiredo, A. M. F., Bender, A. A., 1992. Tectonics and stratigraphy of the East Brazil Rift system: an overview. Tectonophysics 213, 97 - 138.

Demercian, S., Szatmari, P., Cobbold, P.R., 1993. Style and pattern of salt diapirs due to thin-skinned gravitational gliding, Campos and Santos basins, offshore Brazil. Tectonophysics 228, 393-433.

Dengo, D.A., Covey, M.C., 1993. Structure of the Eastern Cordillera of Colombia: Implications for Trap Styles and Regional Tectonics. AAPG Bulletin 77, 1315-1337.

Dias, J.L., 2005. Tectônica, estratigrafia e sedimentação no Andar Aptiano da margem leste brasileira. B. Geoci. Petrobras, Rio de Janeiro v. 13, n. 1, 27 - 25.

Duval, B., Cramez, C., Jackson, M.P.A., 1992. Raft tectonics in the Kwanza Basin, Angola. Marine and Petroleum Geology 9, 389-404.

Fiduk, J.C., Brush, E.R., Anderson, L.E., Gibbs, P.B., Rowan, M.G., 2004. Salt-Sediment Interactions and Hydrocarbon Prospectivity: Concepts, Applications and Case Studies for the 21st Century. Gulf Coast Society of Economic Paleontologists and Mineralogists Foundation, 24th Bob F. Perkins Research Conference Proceedings (CD-ROM). Salt deformation, magmatism, and hydrocarbon prospectivity in the Espírito Santo Basin, offshore Brazil, 370-392.

França, R.L., del Rey, A.C., Tagliari, C.V., Brandão, J.R., Fontanelli, P.R., 2007. Bacia do Espírito Santo. Bol. Geocienc. Petrobras 15, 501 - 509.

Gamboa, D., Alves, T., Cartwright, J., 2011. Distribution and characterization of failed (mega)blocks along salt ridges, southeast Brazil: Implications for vertical fluid flow on continental margins. Journal of Geophysical Research: Solid Earth 116, B08103.

Gamboa, D., Alves, T.M., Cartwright, J., 2012. A submarine channel confluence classification for topographically confined slopes. Marine and Petroleum Geology 35, 176-189.

Gaullier, V., Brun, J.P., Gue´rin, G., Lecanu, H., 1993. Raft tectonics: the effects of residual topography below a salt de´collement. Tectonophysics 228, 363-381.

Isacks, B.L., 1988. Uplift of the Central Andean Plateau and bending of the Bolivian Orocline. Journal of Geophysical Research: Solid Earth 93, 3211-3231.

Jackson, M., Cramez, C., 1989. Seismic recognition of salt welds in salt tectonics regimes, Gulf of Mexico salt tectonics, associated processes and exploration potential: Gulf Coast Section SEPM Foundation 10th Annual Research Conference, pp. 66-71.

Kumar, N., Gamboa, L., Schreiber, B., Mascle, J., 1977. Geologic history and origin of Sao Paulo Plateau (Southeastern Brazilian Margin), comparison with the Angolan margin and the early evolution of the Northern South Atlantic. Supko, PR, Perch-Nielsen, K. (Eds.), 927e945.

Lentini, M.R., Fraser, S.I., Sumner, H.S., Davies, R.J., 2010. Geodynamics of the central South Atlantic conjugate margins: implications for hydrocarbon potential. Petroleum Geoscience 16, 217-229.

Lima, C., 2003. Ongoing compression across South American plate: observations, numerical modelling and some implications for petroleum geology. Geological Society, London, Special Publications 209, 87-100.

Mauduit, T., Guerin, G., Brun, J.P., Lecanu, H., 1997. Raft tectonics: the effects of basal slope angle and sedimentation rate on progressive extension. Journal of Structural Geology 19, 1219-1230.

Mckee, E.H., Noble, D.C., 1982. Miocene volcanism and deformation in the western Cordillera and high plateaus of south-central Peru. Geological Society of America Bulletin 93, 657-662.

Mégard, F., 1984. The Andean orogenic period and its major structures in central and northern Peru. Journal of the Geological Society 141, 893-900.

Mégard, F., Noble, D.C., McKee, E.H., Bellon, H., 1984. Multiple pulses of Neogene compressive deformation in the Ayacucho intermontane basin, Andes of central Peru. Geological Society of America Bulletin 95, 1108-1117.

Mello, M. R., Maxwell, J. R., 1991. Organic geochemical and biological marker characterization of source rocks and oils derived from lacustrine environments in the Brazilian continental margin. In: Katz, B. J. (ed.) Lacustrine Basin Exploration – Case Studies and Modern Analogs. AAPG, Memoir, 50, 77–98.

Mohriak, W.U., 2003. Bacias Sedimentares da Margen Continental Brasileira. Geologia, Tectônica e Recursos Minerais do Brasil, CPRM, São Paulo, Capítulo III In: Bizzi, L. A., Schobbednhaus, C., Vidotti, R. M. & Gonçalves, J. H. (eds), 87 - 165.

Mohriak, W.U., 2005. Interpretação geológica e geofísica da Bacia do Espírito Santo e da região de Ambrolhos: Petrografia, datação radiométrica e visualização sísmica das rochas vulcânicas. . Bol. Geocien. Petrobras 14, 73 - 87.

Mohriak, W.U., Nemcok, M., Enciso, G., 2008. South Atlantic divergen margin evolution: rift□borded uplift and salt tectonics in the basins of Southeastern Brazil. In: R.J. Pankhurst, R.A.J. Trouw, B.B. Brito Neves and M.J. de Wit (Eds.), West Gondwana pre□Cenozoic correlations across the South Atlantic region. Geological Society London, Special Publications 294, 365 - 398.

Mora, A., Parra, M., Strecker, M.R., Kammer, A., Dimaté, C., Rodríguez, F., 2006. Cenozoic contractional reactivation of Mesozoic extensional structures in the Eastern Cordillera of Colombia. Tectonics 25, TC2010, doi: 10.1029/2005TC001854.

Ojeda, H.A.O., 1982. Structural framework, stratigraphy, and evolution of Brazilian marginal basins. AAPG Bulletin 66, 732-749.

Omosanya, K.d.O., Alves, T.M., 2013. Ramps and flats of mass-transport deposits (MTDs) as markers of seafloor strain on the flanks of rising diapirs (Espírito Santo Basin, SE Brazil). Marine Geology 340, 82-97.

Ortiz-Karpf, A., Hodgson, D.M., McCaffrey, W.D., 2015. The role of mass-transport complexes in controlling channel avulsion and the subsequent sediment dispersal patterns on an active margin: The Magdalena Fan, offshore Colombia. Marine and Petroleum Geology 64, 58-75.

Penge, J., Munns, J.W., Taylor, B., Windle, T.M.F., 1999. Rift–raft tectonics: examples of gravitational tectonics from the Zechstein basins of northwest Europe. Geological Society, London, Petroleum Geology Conference series 5, 201-213.

Pilcher, R.S., Murphy, R.T., Ciosek, J.M., 2014. Jurassic raft tectonics in the northeastern Gulf of Mexico. Interpretation 2, SM39-SM55.

Roure, F., Colletta, B., De Toni, B., Loureiro, D., Passalacqua, H., Gou, Y., 1997. Within-plate deformations in the Maracaibo and East Zulia basins, western Venezuela. Marine and Petroleum Geology 14, 139-163.

Rowan, M.G., Jackson, M.P.A., Trudgill, B.D., 1999. Salt-related fault families and fault welds in the northern Gulf of Mexico. AAPG Bulletin 83, 1454-1484.

Rowan, M.G., Lawton, T.F., Giles, K.A., 2012. Anatomy of an exposed vertical salt weld and flanking strata, La Popa Basin, Mexico. Geological Society, London, Special Publications 363, 33-57.

Sarmiento, L.F., Rangel, A., 2004. Petroleum systems of the Upper Magdalena Valley, Colombia. Marine and Petroleum Geology 21, 373-391.

Scheuber, E., Bogdanic, T., Jensen, A., Reutter, K.-J., 1994. Tectonic Development of the North Chilean Andes in Relation to Plate Convergence and Magmatism Since the Jurassic, in: Reutter, K.-J., Scheuber, E., Wigger, P. (Eds.), Tectonics of the Southern Central Andes. Springer Berlin Heidelberg, pp. 121-139.

Vendeville, B.C., 2005. Salt tectonics driven by sediment progradation: Part I—Mechanics and kinematics. AAPG Bulletin 89, 1071-1079.

Vieira, P.E., Bruhn, H.L.C., Santos, C.F., Del Rey, A.C., Alves, R.G., 2007. Golfinho field-discovery, development, and future prospects. Offshore Technology Conference, Houston, Texas.

Figure Captions

Fig. 1 – a) Map of southeast Brazilian margin highlighting the location of the study area (Block BES 100). The map shows the main structural elements that separate Espírito Santo from the Campos and Santos basins. Note the prominent bathymetric high (Abrolhos Plateau) that dominates the northern half of the Espírito Santo Basin, and the presence of an East-West seamount chain (Vitória-Trindade Chain) to the east of the study area. Raft movement in most of the study area was from the northwest and west towards the southeast and east. b) Structural map with interpreted rafts summarising the relative position of rafts in the study area, and highlighting the geometry of North-South Albian rafts on the continental slope of Espírito Santo. Numbers 1 to 4 denote the distinct rafts referred to in the text. c) Interpreted West to East seismic profile highlighting the style of raft tectonics, and geometry of surrounding units, for general context. The top and base of Rafts 1 to 3 are observed in the seismic section. Only the top horizon is observed in Rafts 4 to 6.

Fig. 2 - Seismic profile highlighting the presence of reactivated structures (including local pop-up structures) in the study area. Highlighted are also roller faults (RF), rollover faults (RoF), keystone faults (KF) and reactivated Faults (RvF).

Fig. 3 – a) Correlation panel between the interpreted seismic units and stratigraphic information from the Espírito Santo Basin based on França et al. (2007). Velocity data for ODP Site 516 was taken from Barker et al. (1983). Maximum thickness and depositional environments of the interpreted units are also shown in the figure. b) Schematic representation highlighting the study area on the continental slope of Espírito Santo Basin as modified from Fiduk et al., (2004); Gamboa et al., (2010) and Omosanya and Alves (2013). SR – Syn-Rift sequence, T – Transitional sequence,

ED – Early Drift sequence, LD – Late Drift sequence. The raft tectonics area is located in the proximal extensional domain (dashed square).

Fig. 4 – Simplified schematic evolution of raft tectonics during the Albian-Santonian period in the study area (modified from Duval et al., 1992 and Pilcher et al., 2014). In a first stage (1), early rafts are formed together with extensional faults. In the second stage (2), the post-raft overburden fills the gaps between the rafts. In the last stage (3), the tabular rafts remained isolated become progressively welded on the pre-salt strata. Note the erosion at the end of this stage (Santonian). The salt accumulated into salt rollers, pillows and the rafts growth internally. In the last two stages are observed extensional faults into the post-raft overburden that laterally confined the raft and/or the salt accumulations. The arrows indicate the slope direction in the Espírito Santo Basin (not to scale).

Fig. 5 - Seismic profile highlighting a phase of widespread movement and erosion of rafts at the end of the Cretaceous (Horizons 4 and 5). As with other figures, the seismic profile shows roller faults (RF), rollover faults (RoF), keystone faults (KF) and reactivated faults (RvF). The rafts reactivation is observed on the base Santonian unconformity, showing local pop-up and tight anticlinal structures (square dashed line).

Figure 6 - Seismic profile showing the geometry of collapsed rafts (see Horizon 3 and 4 for reference). As with other figures, the seismic profile shows roller faults (RF), rollover faults (RoF), keystone faults (KF) and reactivated faults (RvF). In this profile, raft 2 collapsed by probable withdrawal of salt from underneath.

Fig. 7 – TWT structure and isochron maps of key horizons in the study area. a) TWT of the top rafts horizon 3, showing the relative location of rafts 1 to 6. b) Isochron map for strata between top rafts

(horizon 3) and base Santonian (horizon 4). c) Isochron map for strata between horizons 4 and 5 (Santonian to top Maastrichtian). Note the marked variations in thickness in these last two maps.

Fig. 8 – Seismic profile highlighting the principal fault families related to raft movements. The figure shows roller faults (RF), rollover faults (RoF), keystone faults (KF) and reactivated faults (RvF). The rafts reactivation is observed on the base Santonian unconformity, showing local pop-up and tight anticlinal structures (square dashed line). The main horizons considered for thickness plots in Figure 12 are also pointed out: base and top rafts, base Santonian and seafloor. The figure include a line (in grey) for horizon reference.

Fig. 9 – Seismic profiles highlighting the major fault types triggered by the movement of rafts and post-raft overburden: a) Roller faults; b) Keystone faults; c) Crystal faults; b) reactivated faults. See Figure 1b for location seismic profiles.

Fig. 10 – Structural maps for key horizons mapped in the study area: a) seafloor, b) Eocene unconformity (horizon 6), c) top Maastrichtian unconformity (horizon 5), d) intra-Santonian unconformity (horizon 4). Note the marked faulting of the mapped horizons.

Fig. 11 – Profile North-South above raft 2. It is showing the elongated body of raft 2. The figure highlights any interpreted horizons together with main sedimentary and structural bodies in the study area. Dashed line (grey) included for reference.

Fig. 12 – Thickness plots for overburden strata above Albian rafts in the study area, acquired in a N-S direction. Data and trend lines refer to the intervals top raft to base Santonian (in grey), base Santonian to seafloor (dashed line, black), and total overburden thickness above Albian rafts (black). The graphs highlight the existence of thicker overburden units towards the central region in

rafts 1, 5 and 6. Conversely, rafts 2, 3 and 4 show the thickest overburden units to the north of the study area. This character contrasts with highest degree of internal deformation recorded in the northern and central parts of the interpreted rafts, as explained in more detail in the text.

Fig. 13 – a) Amplitude map from 25 ms-thick window below the base Santonian showing the main fault families that intersect Horizon 4 (base Santonian); b) interpretation based on the amplitude map (Fig. 13a) highlighting the faults families; c) block diagram through segment A-B (Fig. 13a), with ~5x vertical exaggeration. It shows rafts 2, 4 and 5, and the main roller faults adjacent to the rafts.

Fig. 14 – a) Uninterpreted and b) interpreted West to East seismic profile showing gentle internal strata growth in raft 2. Note the presence of growth raft strata above the salt roller to the east, and the initiation of a triangular-shaped structure above raft 2. The raft is lateral confined by salt structures, salt roller to the west and salt pillow to the east.

Fig. 15 – a) Uninterpreted and b) interpreted West to East seismic profile showing collapsed lateral part of raft 2, listric normal faults and raft welded on the pre-salt units.

Fig. 16 - a) Uninterpreted and b) interpreted West to East seismic profile showing the structural deformation in raft 2. Deformation styles include the tilting of flanking strata, ramping up on the salt structures and collapse of the central part of raft 2, lateral constrained by extensional faults and welded on the pre-salt units. In the figure is highlighted the thickness (m) between the i) top raft to base Santonian and ii) base Santonian to seafloor, for reference.

Fig. 17 - Conceptual schematic evolution of rafts in the study area, highlighting the effect of salt pillow growth on the structural compartmentalisation of Albian (and younger) strata in the Espírito

Santo Basin. Fault systems in the figure are associated with different styles of raft deformation, as described in this paper. Modified from Alves (2012).

Figure 18 - Uninterpreted and b) interpreted West to East seismic profile highlighting the presence of fluid-flow features above listric faults in raft 3. Fluid putatively migrates from pre-salt and intra-raft units to accumulate above the listric faults in Late Cretaceous strata. Note the presence of propagated Rollover faults into Cenozoic units to the East of raft 3.

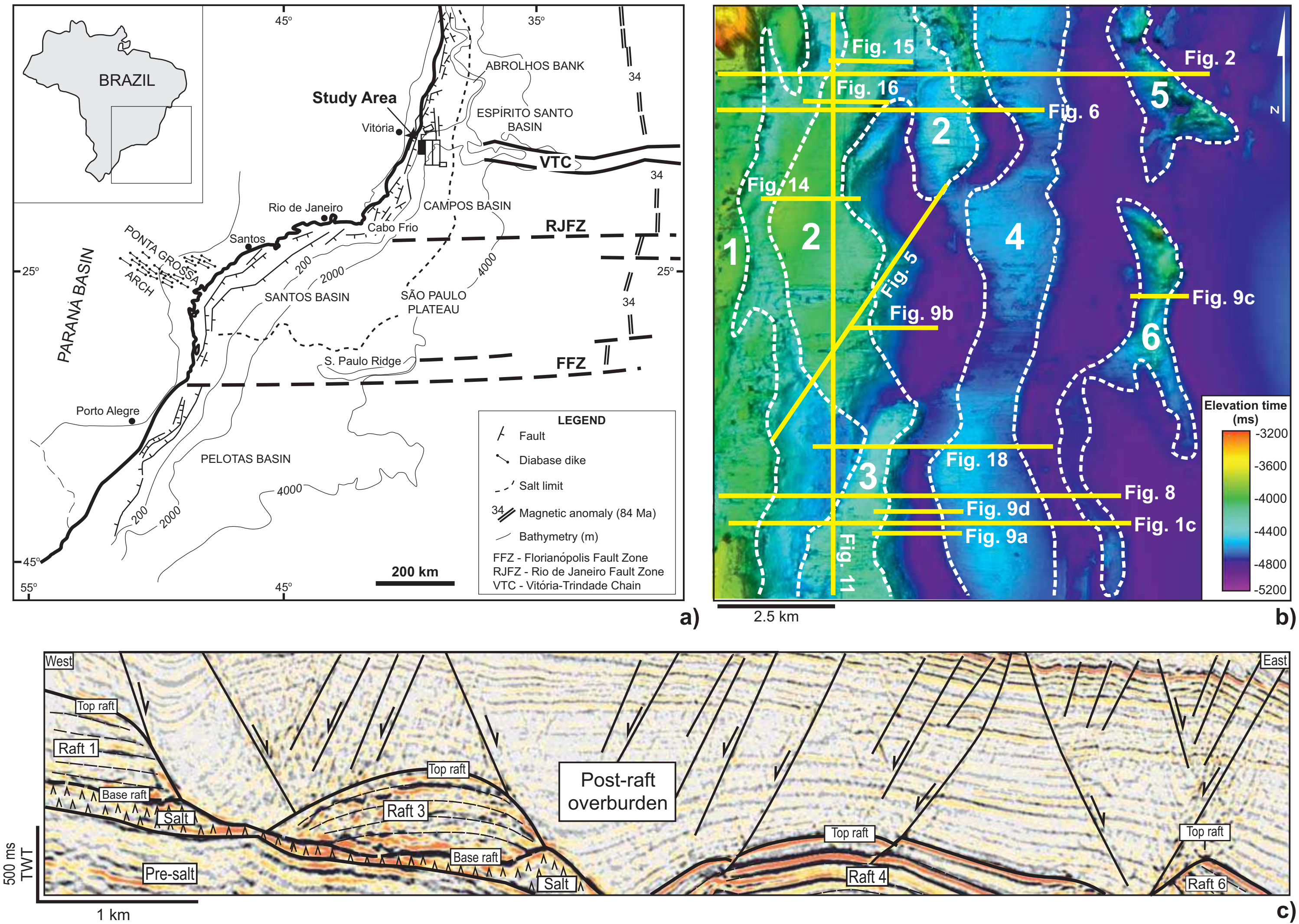
BRAZIL
Study Area
Vitória
ABROLHOS BANK
ESPÍRITO SANTO BASIN
VTC
CAMPOS BASIN
Rio de Janeiro
Cabo Frio
RJFZ
Santos
PONTA GROSSA ARCH
PARANÁ BASIN
SANTOS BASIN
SÃO PAULO PLATEAU
S. Paulo Ridge
FFZ
Porto Alegre
PELOTAS BASIN
LEGEND
Fault
Diabase dike
Salt limit
Magnetic anomaly (84 Ma)
Bathymetry (m)
FFZ - Florianópolis Fault Zone
RJFZ - Rio de Janeiro Fault Zone
VTC - Vitória-Trindade Chain
200 km
a)
Fig. 15
Fig. 16
Fig. 2
Fig. 6
Fig. 14
Fig. 5
Fig. 9b
Fig. 9c
Fig. 18
Fig. 8
Fig. 9d
Fig. 1c
Fig. 9a
Fig. 11
Elevation time (ms)
2.5 km
b)
West
East
Top raft
Raft 1
Base raft
Salt
Pre-salt
Raft 3
Post-raft overburden
Raft 4
Raft 6
500 ms TWT
1 km
c)

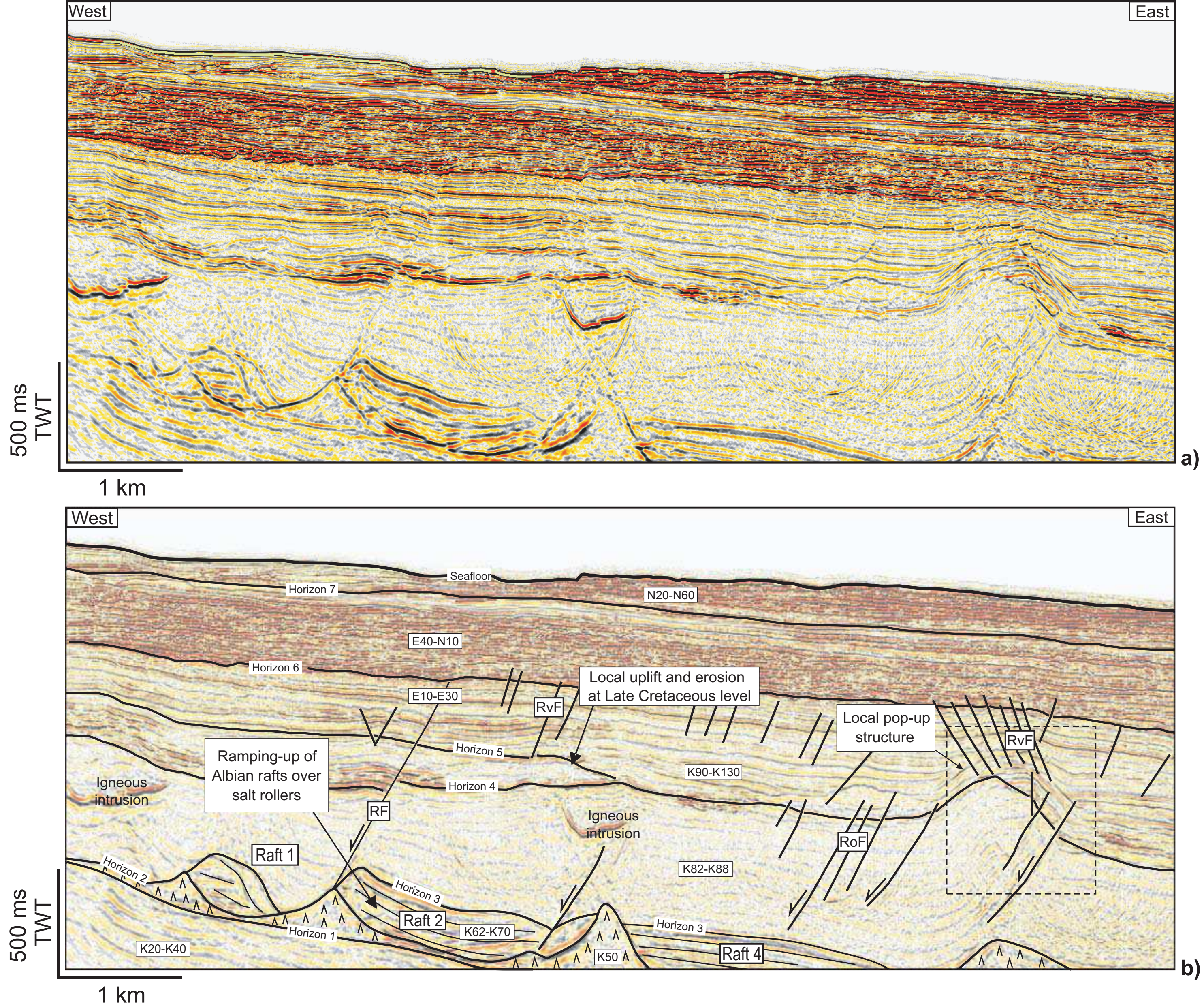
West
East
500 ms TWT
1 km
a)
West
East
Seafloor
Horizon 7
N20-N60
E40-N10
Horizon 6
E10-E30
RvF
Local uplift and erosion at Late Cretaceous level
Local pop-up structure
RvF
Horizon 5
Horizon 4
K90-K130
Igneous intrusion
Ramping-up of Albian rafts over salt rollers
RF
Igneous intrusion
RoF
Raft 1
K82-K88
Horizon 2
Horizon 3
Raft 2
K62-K70
Horizon 3
Horizon 1
Raft 4
K20-K40
K50
500 ms TWT
1 km
b)

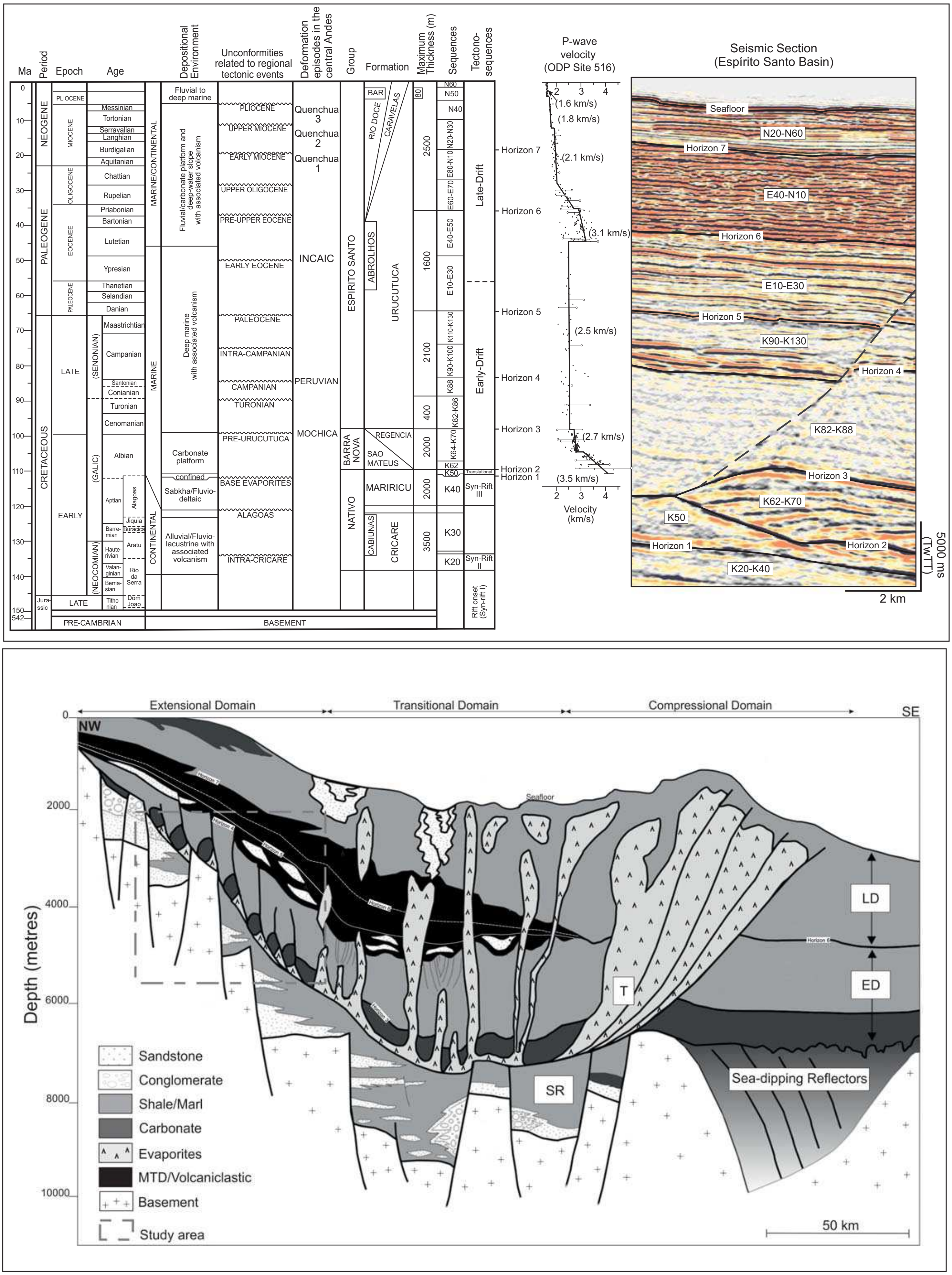

Ma
Period
Epoch
Age
Depositional Environment
Unconformities related to regional tectonic events
Deformation episodes in the central Andes
Group
Formation
Maximum Thickness (m)
Sequences
Tectono-sequences
NEOGENE
PALEOGENE
CRETACEOUS
Jurassic
PLIOCENE
MIOCENE
OLIGOCENE
EOCENE
PALEOCENE
LATE
EARLY
Messinian
Tortonian
Serravalian
Langhian
Burdigalian
Aquitanian
Chattian
Rupelian
Priabonian
Bartonian
Lutetian
Ypresian
Thanetian
Selandian
Danian
Maastrichtian
Campanian
Santonian
Coniacian
Turonian
Cenomanian
Albian
Aptian
Barremian
Hauterivian
Valanginian
Berriasian
Tithonian
(SENONIAN)
(GALIC)
(NEOCOMIAN)
Alagoas
Jiquia
Buracica
Aratu
Rio da Serra
Dom João
PRE-CAMBRIAN
BASEMENT
MARINE/CONTINENTAL
MARINE
CONTINENTAL
Fluvial to deep marine
Fluvial/carbonate platform and deep-water slope with associated volcanism
Deep marine with associated volcanism
Carbonate platform
confined
Sabkha/Fluvio-deltaic
Alluvial/Fluvio-lacustrine with associated volcanism
PLIOCENE
UPPER MIOCENE
EARLY MIOCENE
UPPER OLIGOCENE
PRE-UPPER EOCENE
EARLY EOCENE
PALEOCENE
INTRA-CAMPANIAN
CAMPANIAN
TURONIAN
PRE-URUCUTUCA
BASE EVAPORITES
ALAGOAS
INTRA-CRICARE
Quenchua 3
Quenchua 2
Quenchua 1
INCAIC
PERUVIAN
MOCHICA
ESPIRITO SANTO
BARRA NOVA
NATIVO
BAR
RIO DOCE
CARAVELAS
ABROLHOS
URUCUTUCA
REGENCIA
SAO MATEUS
MARIRICU
CABIUNAS
CRICARE
80
2500
1600
2100
400
2000
2000
3500
N60
N50
N40
N20-N30
E80-N10
E60-E70
E40-E50
E10-E30
K110-K130
K90-K100
K88
K82-K86
K64-K70
K62
K50
K40
K30
K20
Late-Drift
Early-Drift
Translational
Syn-Rift III
Syn-Rift II
Rift onset (Syn-rift I)
Horizon 7
Horizon 6
Horizon 5
Horizon 4
Horizon 3
Horizon 2
Horizon 1
P-wave velocity (ODP Site 516)
(1.6 km/s)
(1.8 km/s)
(2.1 km/s)
(3.1 km/s)
(2.5 km/s)
(2.7 km/s)
(3.5 km/s)
Velocity (km/s)
Seismic Section (Espírito Santo Basin)
Seafloor
N20-N60
E40-N10
E10-E30
K90-K130
K82-K88
K62-K70
K50
K20-K40
5000 ms (TwTT)
2 km
Extensional Domain
Transitional Domain
Compressional Domain
NW
SE
Seafloor
Depth (metres)
LD
ED
T
SR
Sea-dipping Reflectors
Sandstone
Conglomerate
Shale/Marl
Carbonate
Evaporites
MTD/Volcaniclastic
Basement
Study area
50 km

a)

b)

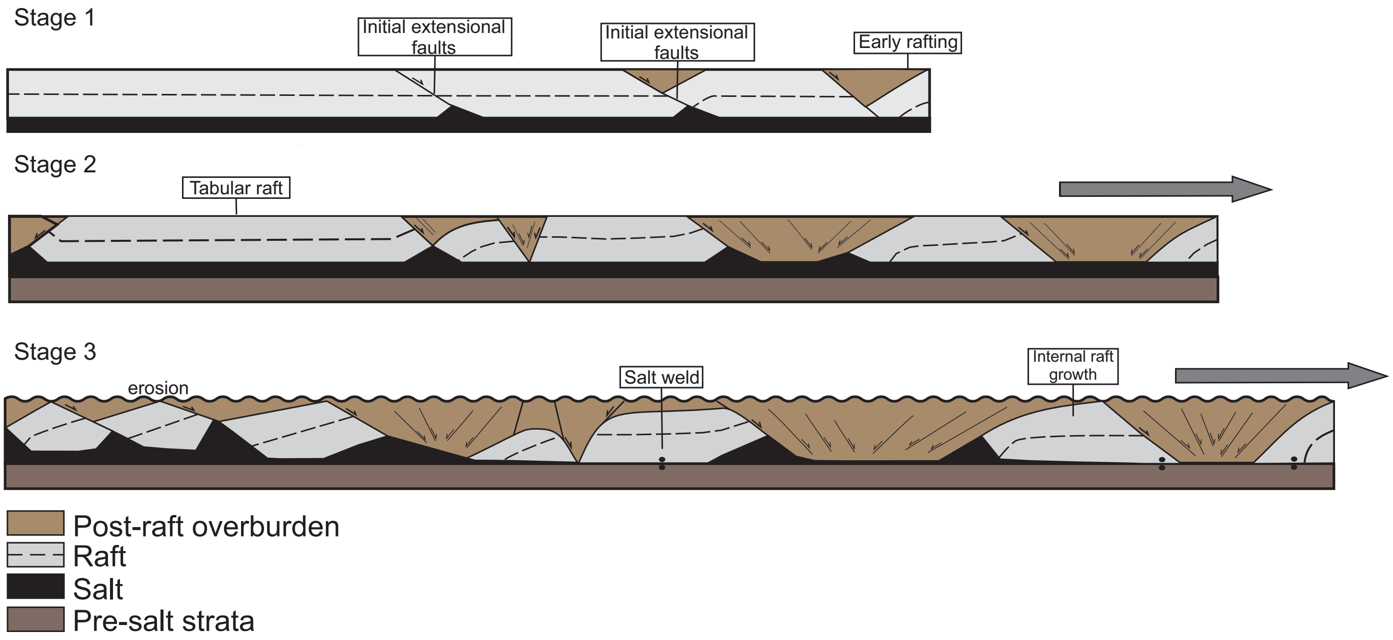

Stage 1
Initial extensional faults
Initial extensional faults
Early rafting
Stage 2
Tabular raft
Stage 3
erosion
Salt weld
Internal raft growth
Post-raft overburden
Raft
Salt
Pre-salt strata

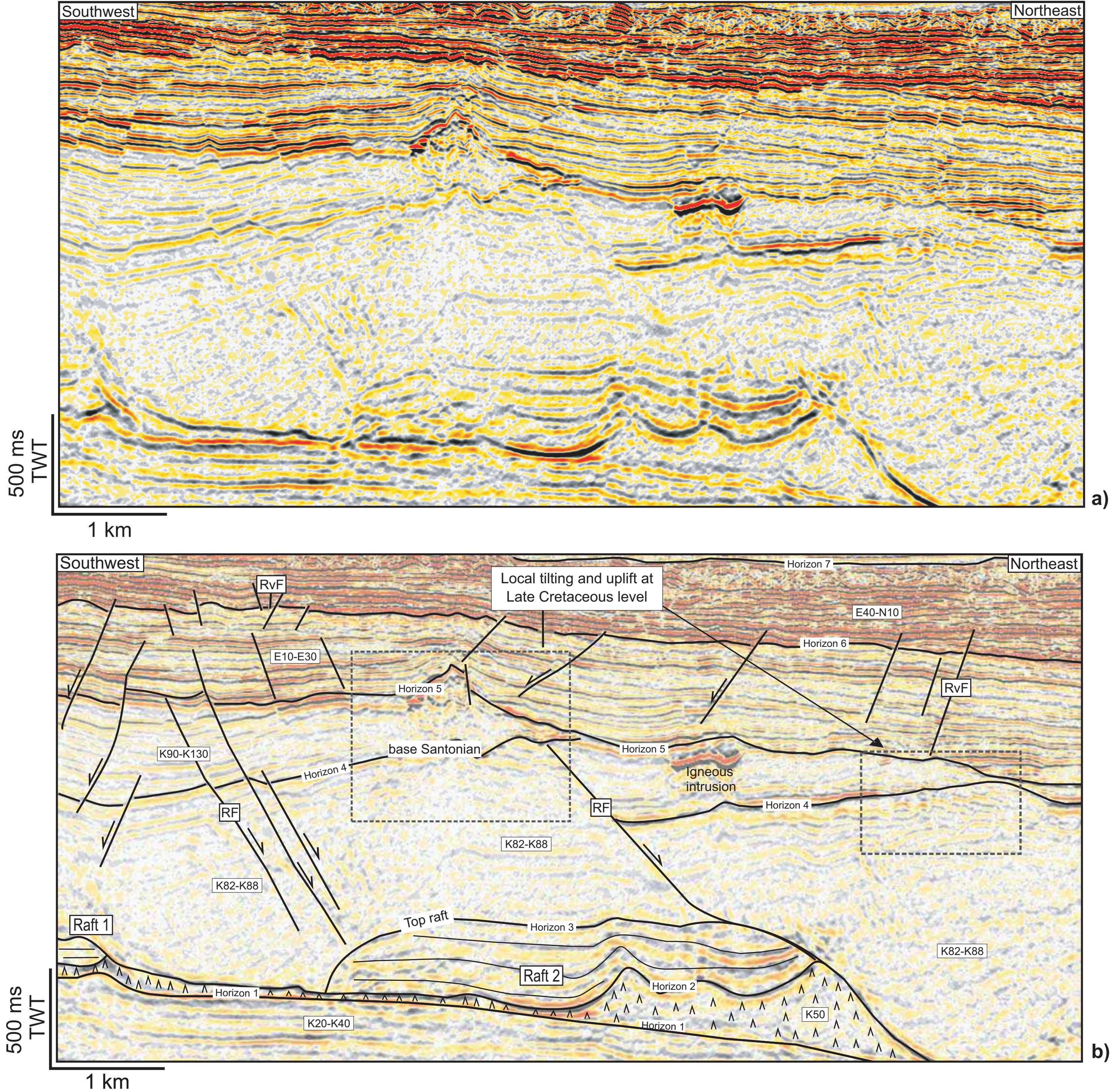
Southwest
Northeast
500 ms TWT
1 km
a)
Southwest
Northeast
Horizon 7
Local tilting and uplift at Late Cretaceous level
RvF
E40-N10
Horizon 6
E10-E30
Horizon 5
RvF
K90-K130
base Santonian
Horizon 5
Igneous intrusion
Horizon 4
Horizon 4
RF
RF
K82-K88
K82-K88
Raft 1
Top raft
Horizon 3
K82-K88
Raft 2
Horizon 2
Horizon 1
K50
K20-K40
Horizon 1
500 ms TWT
1 km
b)

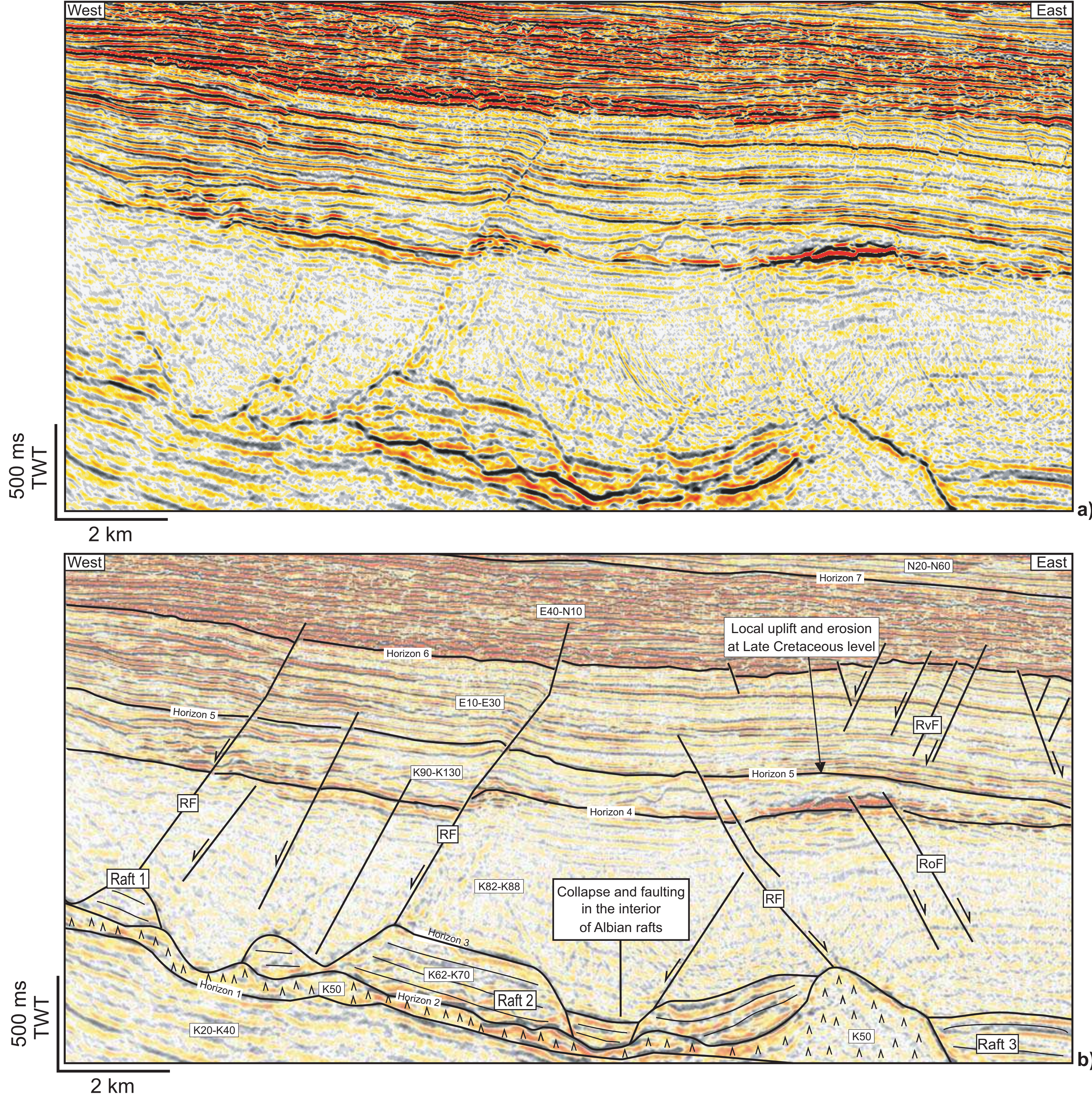

West
East
500 ms TWT
2 km
a)
West
East
N20-N60
Horizon 7
E40-N10
Local uplift and erosion at Late Cretaceous level
Horizon 6
E10-E30
Horizon 5
RvF
RF
K90-K130
Horizon 5
Horizon 4
RF
RoF
Raft 1
K82-K88
Collapse and faulting in the interior of Albian rafts
RF
Horizon 3
K62-K70
Horizon 1
K50
Horizon 2
Raft 2
K50
K20-K40
Raft 3
500 ms TWT
2 km
b)

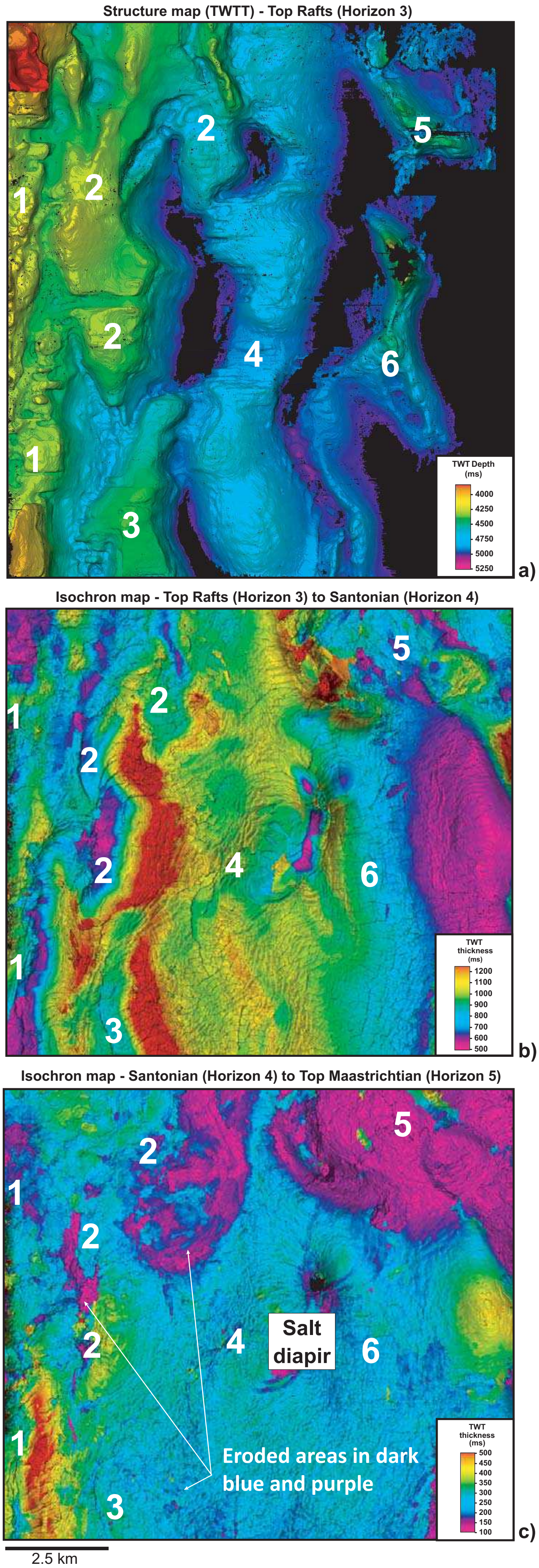
Structure map (TWTT) - Top Rafts (Horizon 3)
1
2
2
2
1
3
4
5
6
TWT Depth (ms)
4000
4250
4500
4750
5000
5250
a)
Isochron map - Top Rafts (Horizon 3) to Santonian (Horizon 4)
1
2
2
2
1
3
4
5
6
TWT thickness (ms)
1200
1100
1000
900
800
700
600
500
b)
Isochron map - Santonian (Horizon 4) to Top Maastrichtian (Horizon 5)
1
2
2
2
1
3
4
5
6
Salt diapir
Eroded areas in dark blue and purple
TWT thickness (ms)
500
450
400
350
300
250
200
150
100
c)
2.5 km

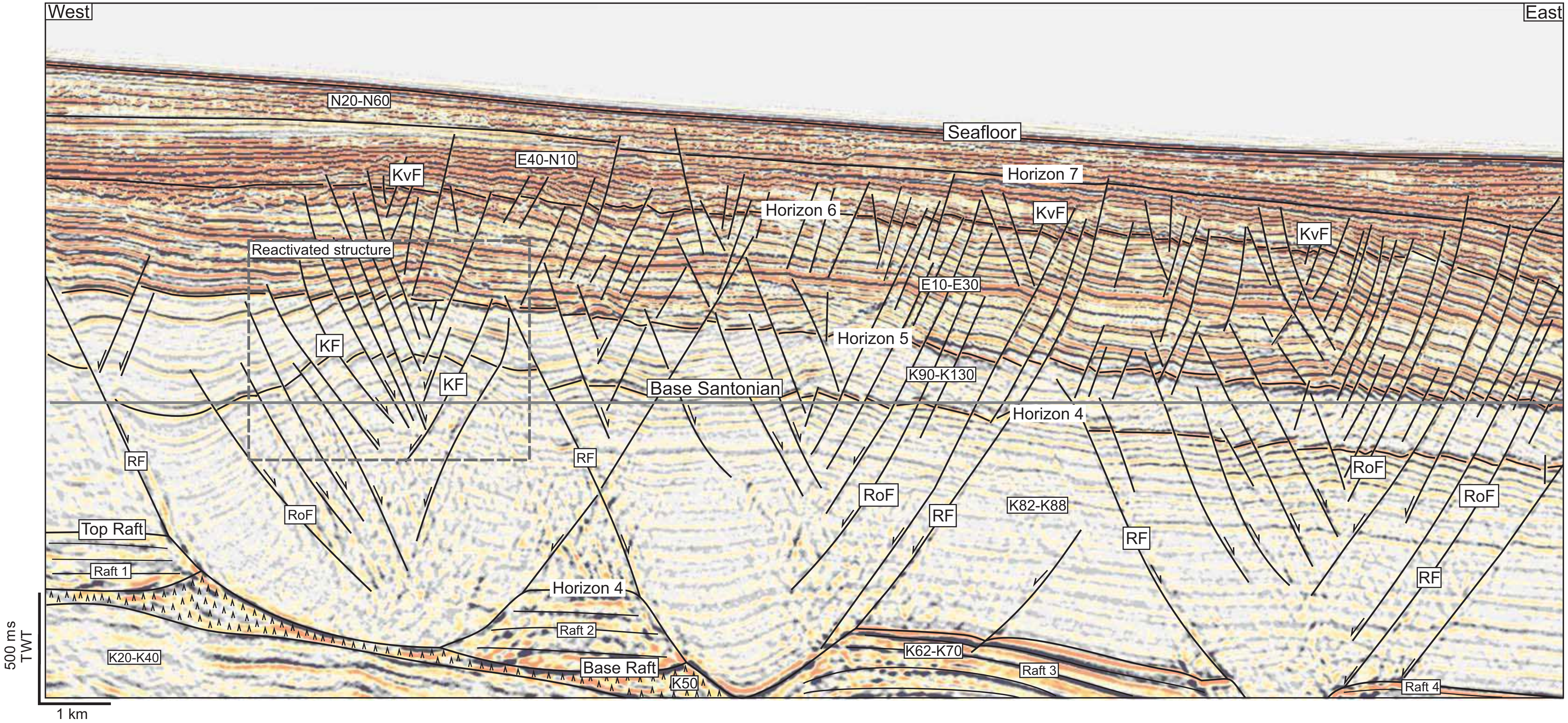

West
East
N20-N60
Seafloor
E40-N10
KvF
Horizon 7
Horizon 6
KvF
KvF
Reactivated structure
E10-E30
KF
Horizon 5
KF
K90-K130
Base Santonian
Horizon 4
RF
RF
RoF
RoF
RF
K82-K88
RF
RoF
RoF
RF
Top Raft
Raft 1
Horizon 4
Raft 2
K62-K70
Raft 3
K20-K40
Base Raft
K50
Raft 4
500 ms
TWT
1 km

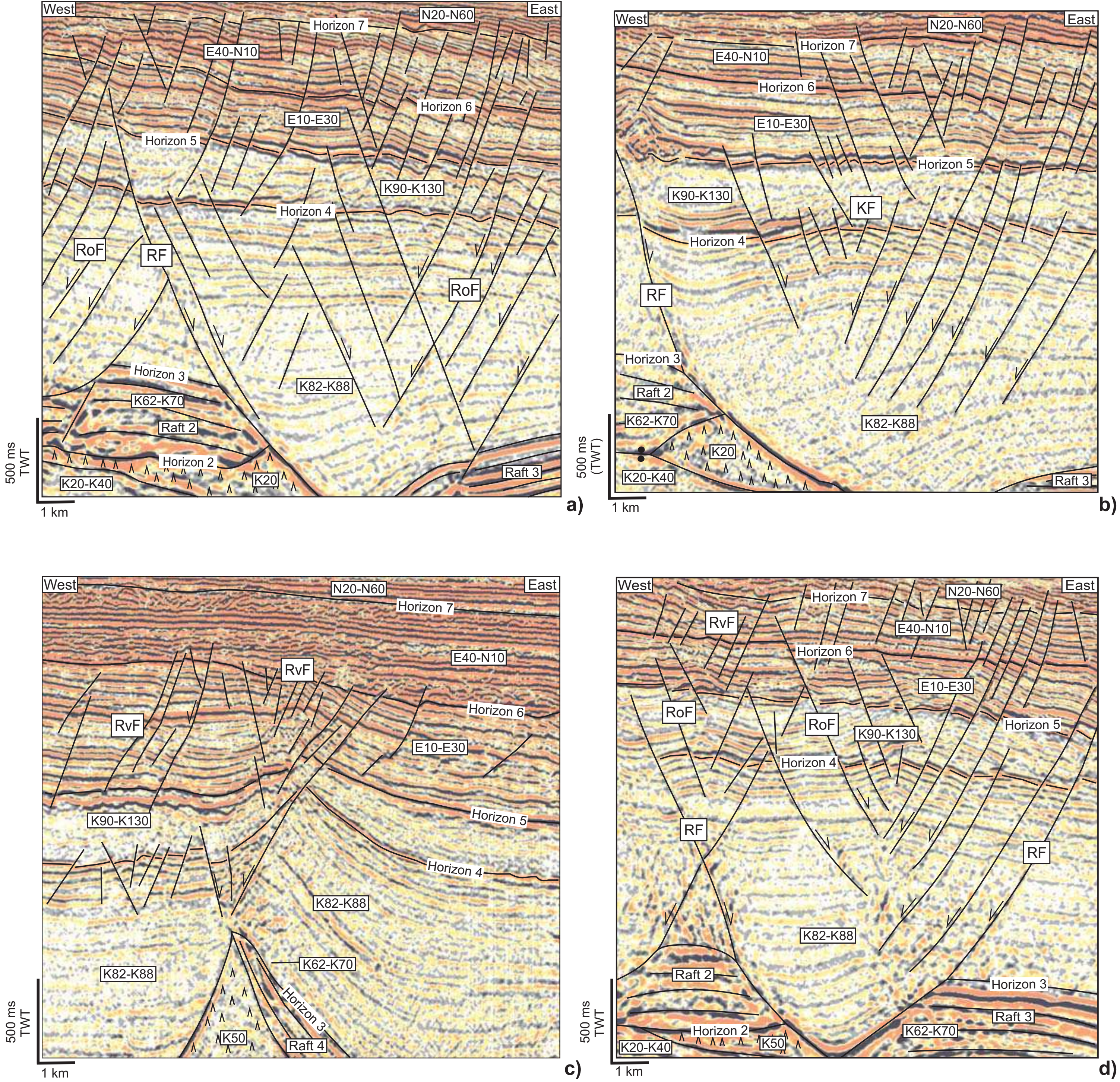

West
East
N20-N60
Horizon 7
E40-N10
Horizon 6
E10-E30
Horizon 5
K90-K130
Horizon 4
RoF
RF
RoF
Horizon 3
K62-K70
K82-K88
Raft 2
Horizon 2
K20-K40
K20
Raft 3
500 ms
TWT
1 km
a)
West
East
N20-N60
Horizon 7
E40-N10
Horizon 6
E10-E30
Horizon 5
K90-K130
KF
Horizon 4
RF
Horizon 3
Raft 2
K62-K70
K20
K20-K40
K82-K88
Raft 3
500 ms
(TWT)
1 km
b)
West
East
N20-N60
Horizon 7
E40-N10
RvF
RvF
Horizon 6
E10-E30
K90-K130
Horizon 5
Horizon 4
K82-K88
K62-K70
K82-K88
Horizon 3
K50
Raft 4
500 ms
TWT
1 km
c)
West
East
Horizon 7
N20-N60
RvF
E40-N10
Horizon 6
E10-E30
RoF
RoF
K90-K130
Horizon 5
Horizon 4
RF
RF
K82-K88
Raft 2
Horizon 3
Raft 3
Horizon 2
K50
K62-K70
K20-K40
500 ms
TWT
1 km
d)

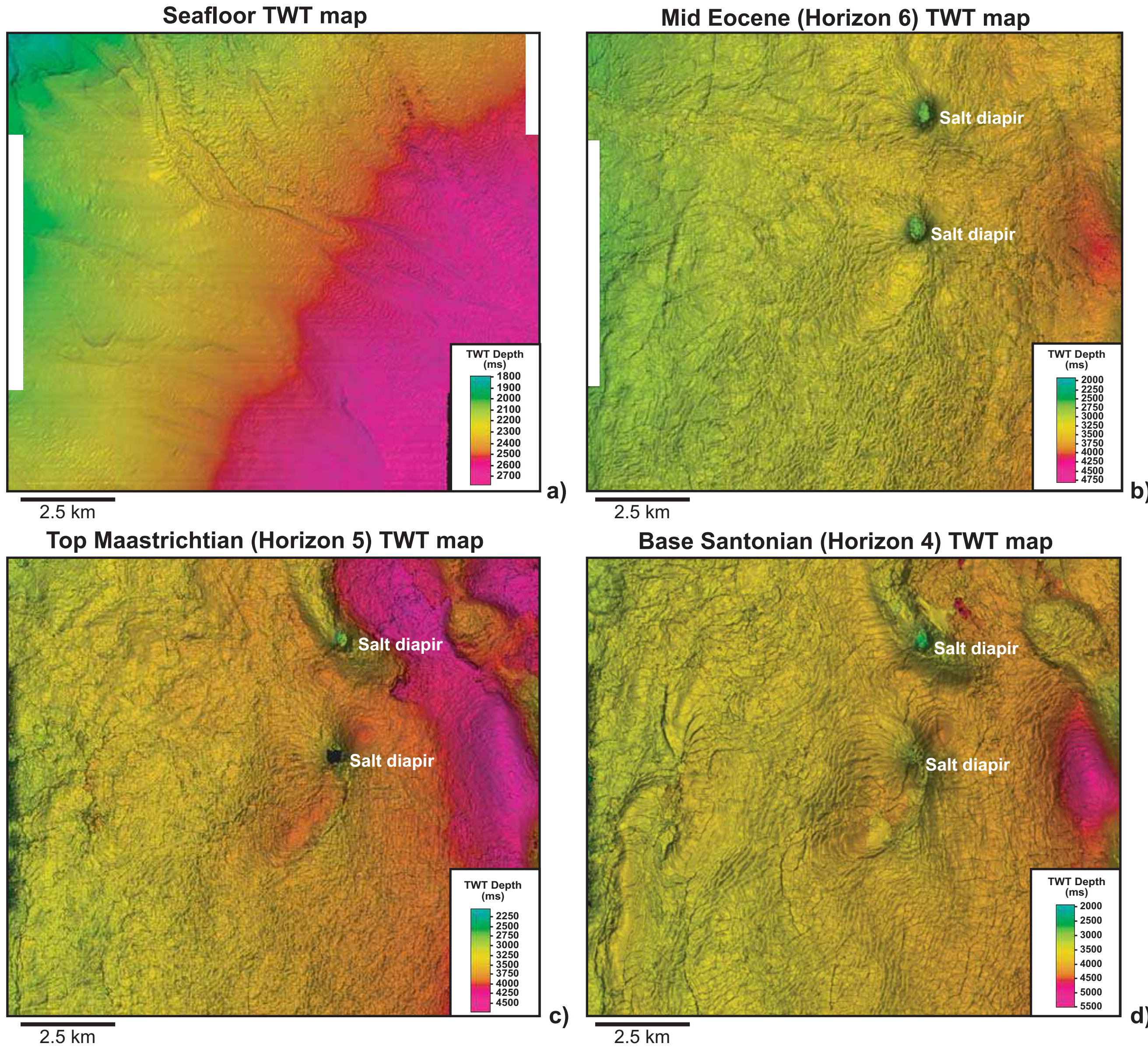
Seafloor TWT map
TWT Depth (ms)
1800
1900
2000
2100
2200
2300
2400
2500
2600
2700
2.5 km
a)
Mid Eocene (Horizon 6) TWT map
Salt diapir
Salt diapir
TWT Depth (ms)
2000
2250
2500
2750
3000
3250
3500
3750
4000
4250
4500
4750
2.5 km
b)
Top Maastrichtian (Horizon 5) TWT map
Salt diapir
Salt diapir
TWT Depth (ms)
2250
2500
2750
3000
3250
3500
3750
4000
4250
4500
2.5 km
c)
Base Santonian (Horizon 4) TWT map
Salt diapir
Salt diapir
TWT Depth (ms)
2000
2500
3000
3500
4000
4500
5000
5500
2.5 km
d)

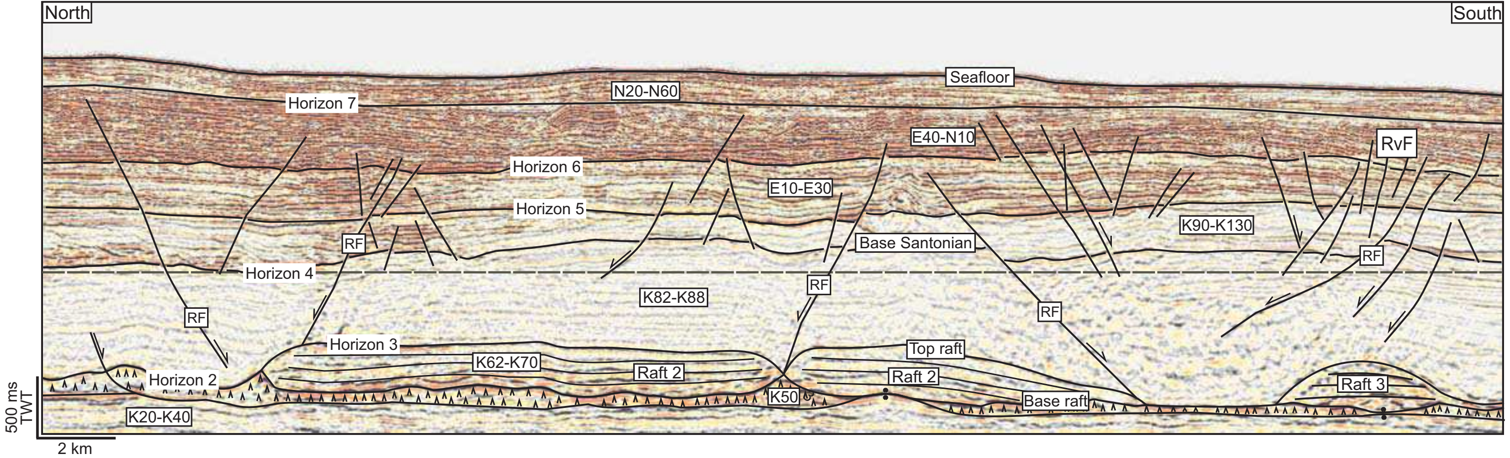
North
South
Seafloor
N20-N60
Horizon 7
E40-N10
RvF
Horizon 6
E10-E30
Horizon 5
K90-K130
Base Santonian
RF
Horizon 4
K82-K88
Horizon 3
Top raft
K62-K70
Raft 2
Horizon 2
Base raft
Raft 3
K50
K20-K40
500 ms TWT
2 km

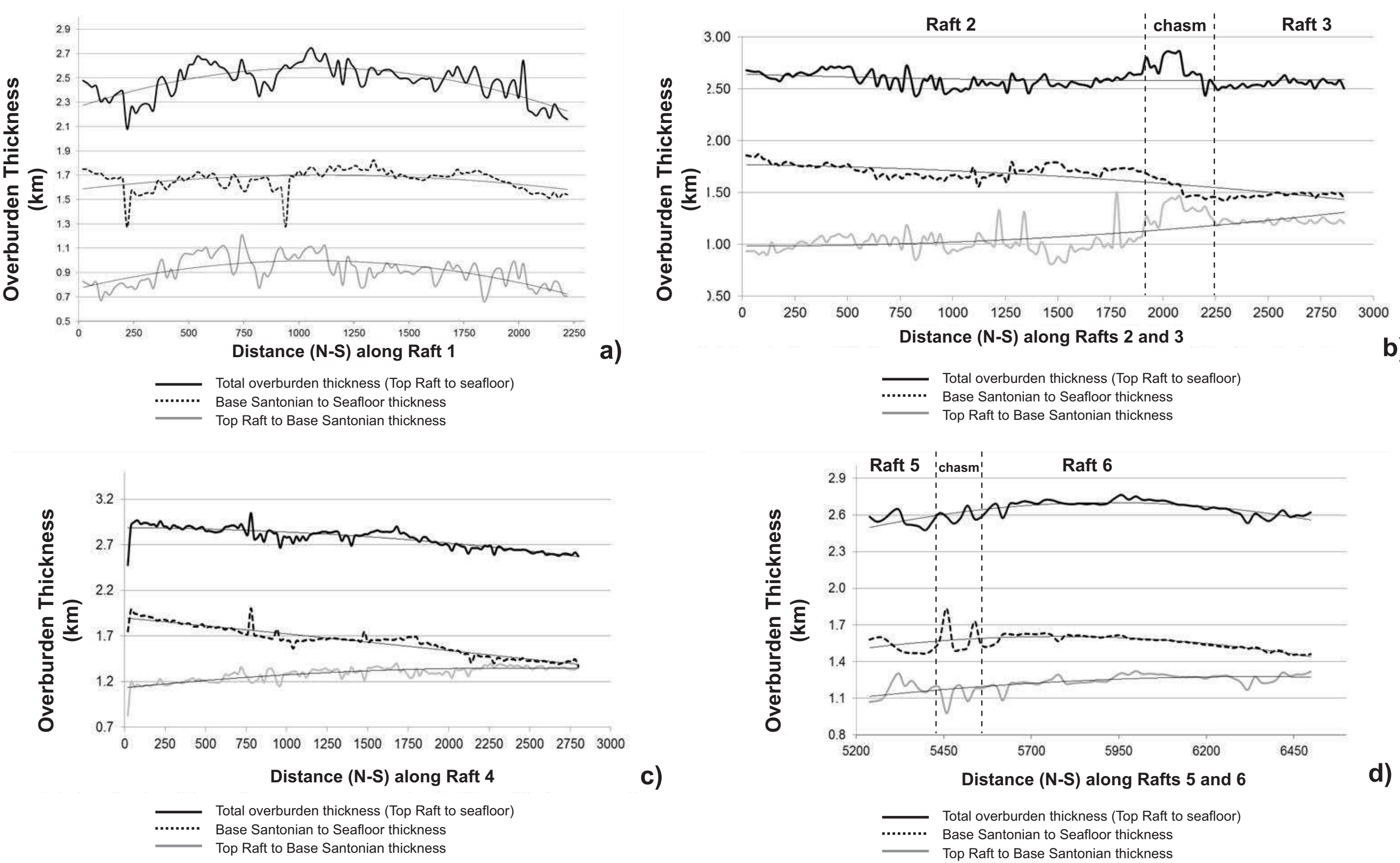

Overburden Thickness (km)
2.9
2.7
2.5
2.3
2.1
1.9
1.7
1.5
1.3
1.1
0.9
0.7
0.5
0
250
500
750
1000
1250
1500
1750
2000
2250
Distance (N-S) along Raft 1
a)
Total overburden thickness (Top Raft to seafloor)
Base Santonian to Seafloor thickness
Top Raft to Base Santonian thickness
Raft 2
chasm
Raft 3
Overburden Thickness (km)
3.00
2.50
2.00
1.50
1.00
0.50
0
250
500
750
1000
1250
1500
1750
2000
2250
2500
2750
3000
Distance (N-S) along Rafts 2 and 3
b)
Total overburden thickness (Top Raft to seafloor)
Base Santonian to Seafloor thickness
Top Raft to Base Santonian thickness
Overburden Thickness (km)
3.2
2.7
2.2
1.7
1.2
0.7
0
250
500
750
1000
1250
1500
1750
2000
2250
2500
2750
3000
Distance (N-S) along Raft 4
c)
Total overburden thickness (Top Raft to seafloor)
Base Santonian to Seafloor thickness
Top Raft to Base Santonian thickness
Raft 5
chasm
Raft 6
Overburden Thickness (km)
2.9
2.6
2.3
2.0
1.7
1.4
1.1
0.8
5200
5450
5700
5950
6200
6450
Distance (N-S) along Rafts 5 and 6
d)
Total overburden thickness (Top Raft to seafloor)
Base Santonian to Seafloor thickness
Top Raft to Base Santonian thickness

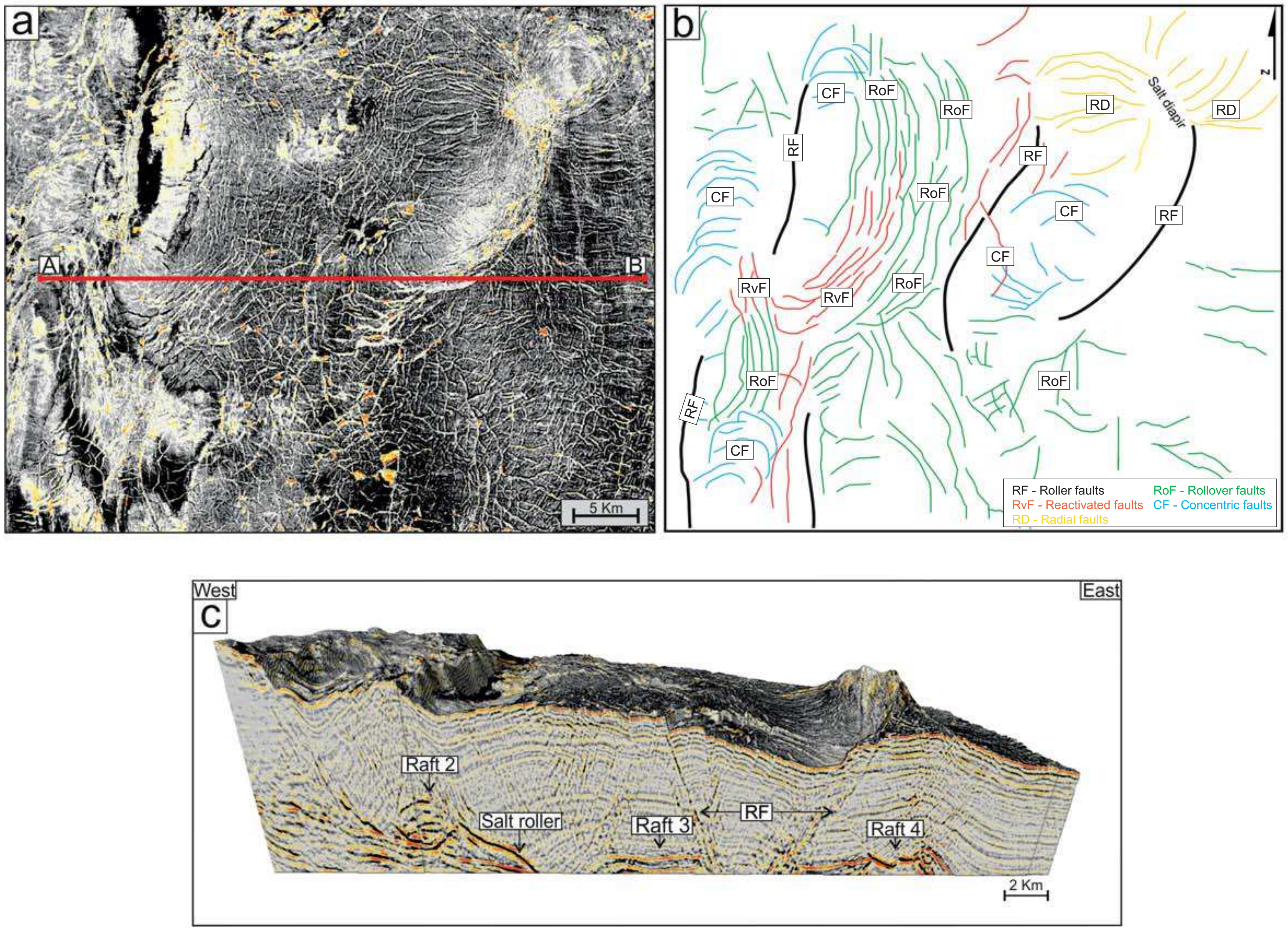
a
A
B
5 Km
b
CF
RoF
RoF
RD
Salt diapir
RD
RF
RF
CF
RoF
CF
RF
CF
RvF
RvF
RoF
RoF
RF
RoF
CF
RF - Roller faults
RoF - Rollover faults
RvF - Reactivated faults
CF - Concentric faults
RD - Radial faults
c
West
East
Raft 2
Salt roller
Raft 3
RF
Raft 4
2 Km

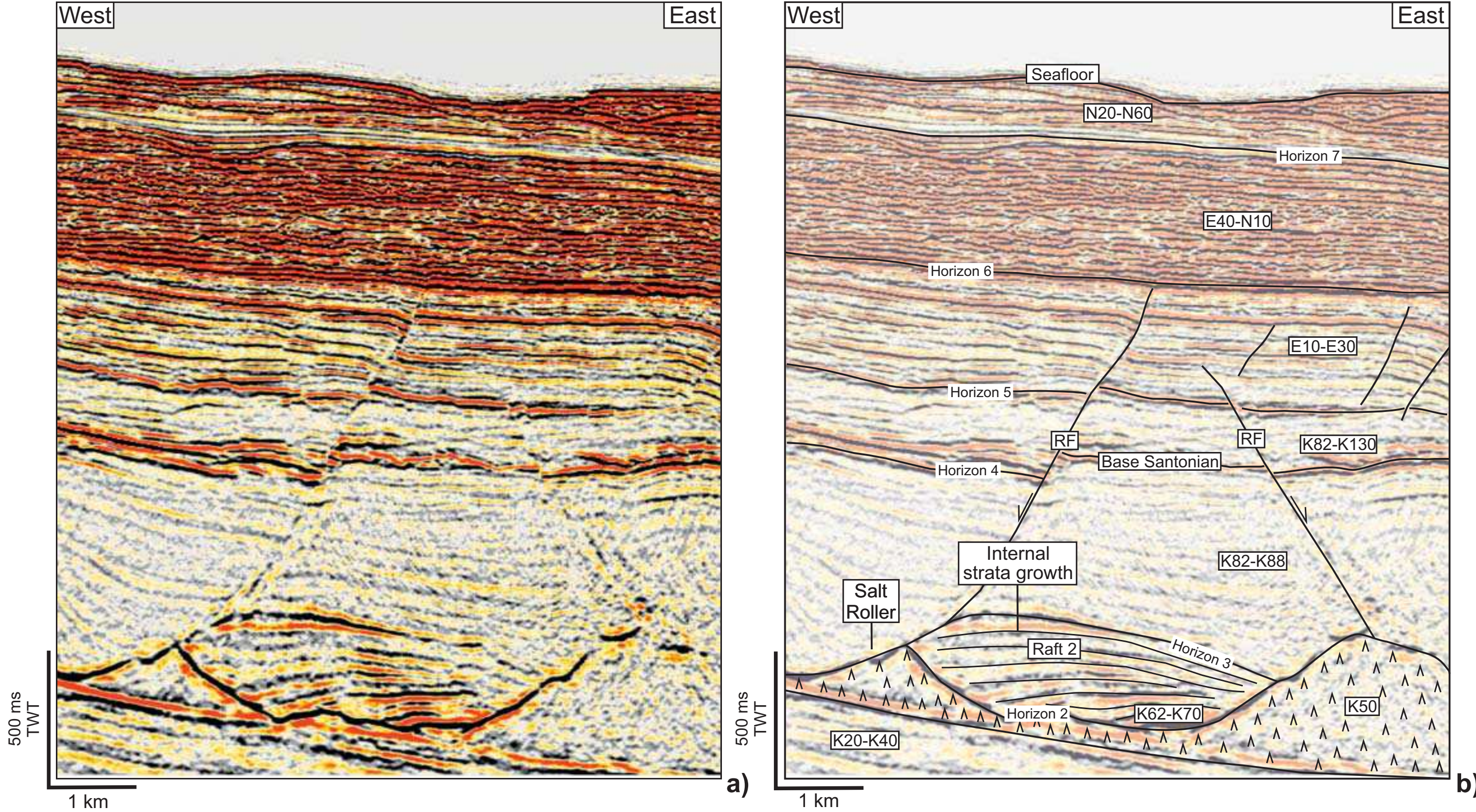
West
East
500 ms TWT
1 km
a)
West
East
Seafloor
N20-N60
Horizon 7
E40-N10
Horizon 6
E10-E30
Horizon 5
RF
RF
K82-K130
Horizon 4
Base Santonian
Internal strata growth
K82-K88
Salt Roller
Raft 2
Horizon 3
Horizon 2
K62-K70
K50
K20-K40
500 ms TWT
1 km
b)

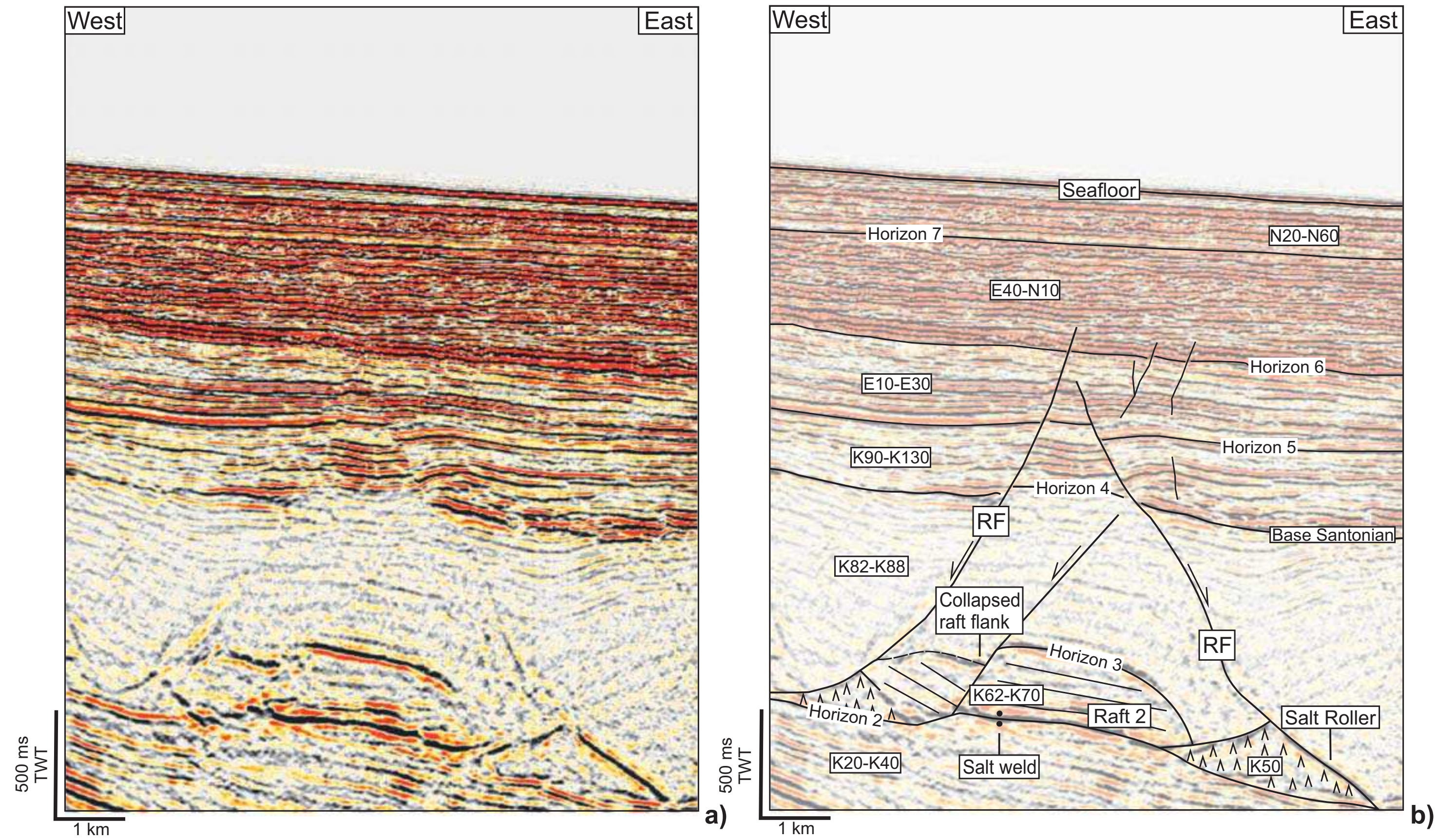
West
East
500 ms TWT
1 km
a)
West
East
Seafloor
Horizon 7
N20-N60
E40-N10
Horizon 6
E10-E30
Horizon 5
K90-K130
Horizon 4
RF
Base Santonian
K82-K88
Collapsed raft flank
Horizon 3
RF
K62-K70
Horizon 2
Raft 2
Salt Roller
K20-K40
Salt weld
K50
500 ms TWT
1 km
b)

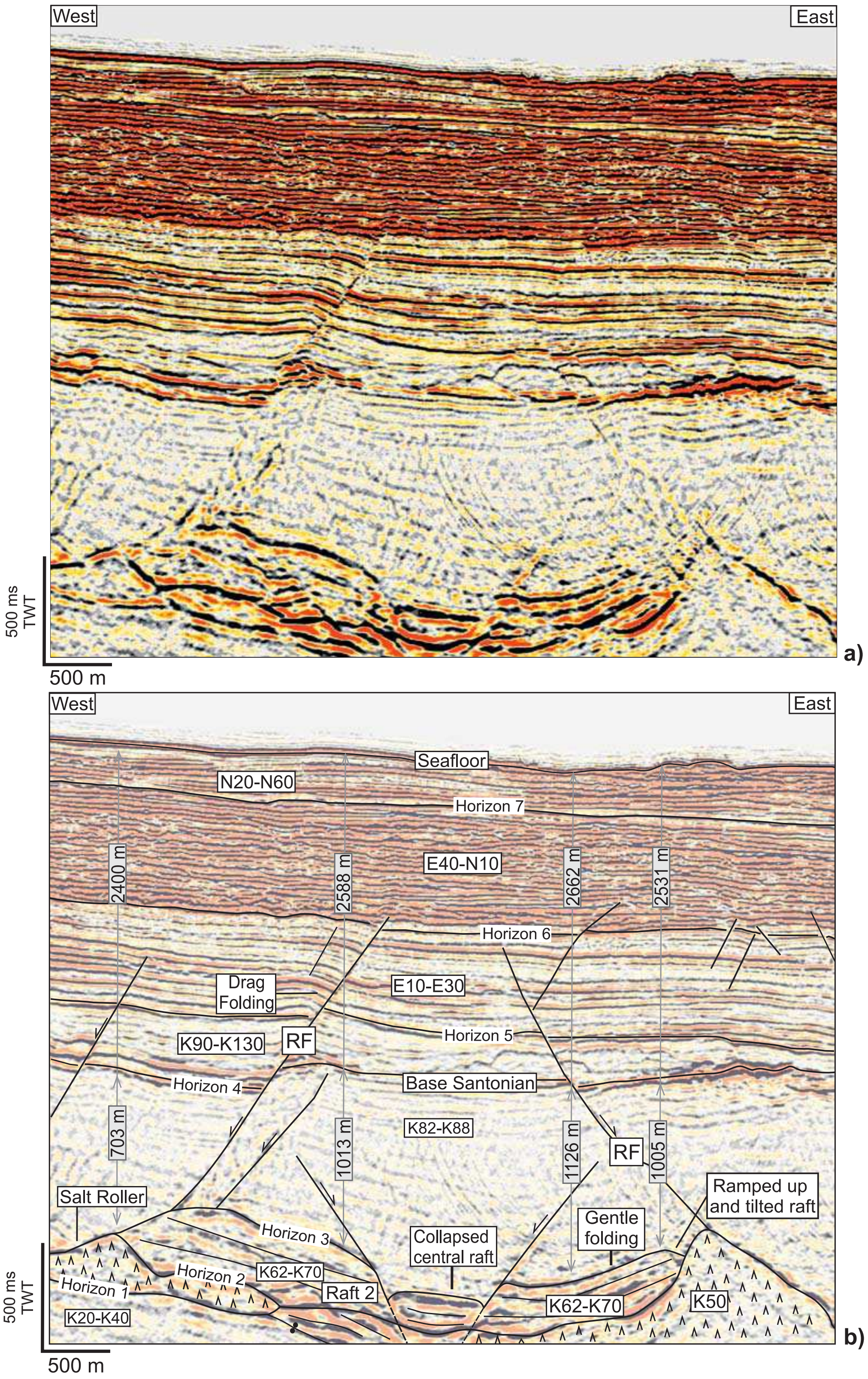
West
East
500 ms
TWT
500 m
a)
West
East
Seafloor
N20-N60
Horizon 7
E40-N10
2400 m
2588 m
2662 m
2531 m
Horizon 6
Drag
Folding
E10-E30
Horizon 5
K90-K130
RF
Horizon 4
Base Santonian
K82-K88
703 m
1013 m
1126 m
1005 m
RF
Salt Roller
Ramped up
and tilted raft
Gentle
folding
Horizon 3
Collapsed
central raft
Horizon 2
K62-K70
Raft 2
Horizon 1
K62-K70
K50
K20-K40
500 ms
TWT
500 m
b)

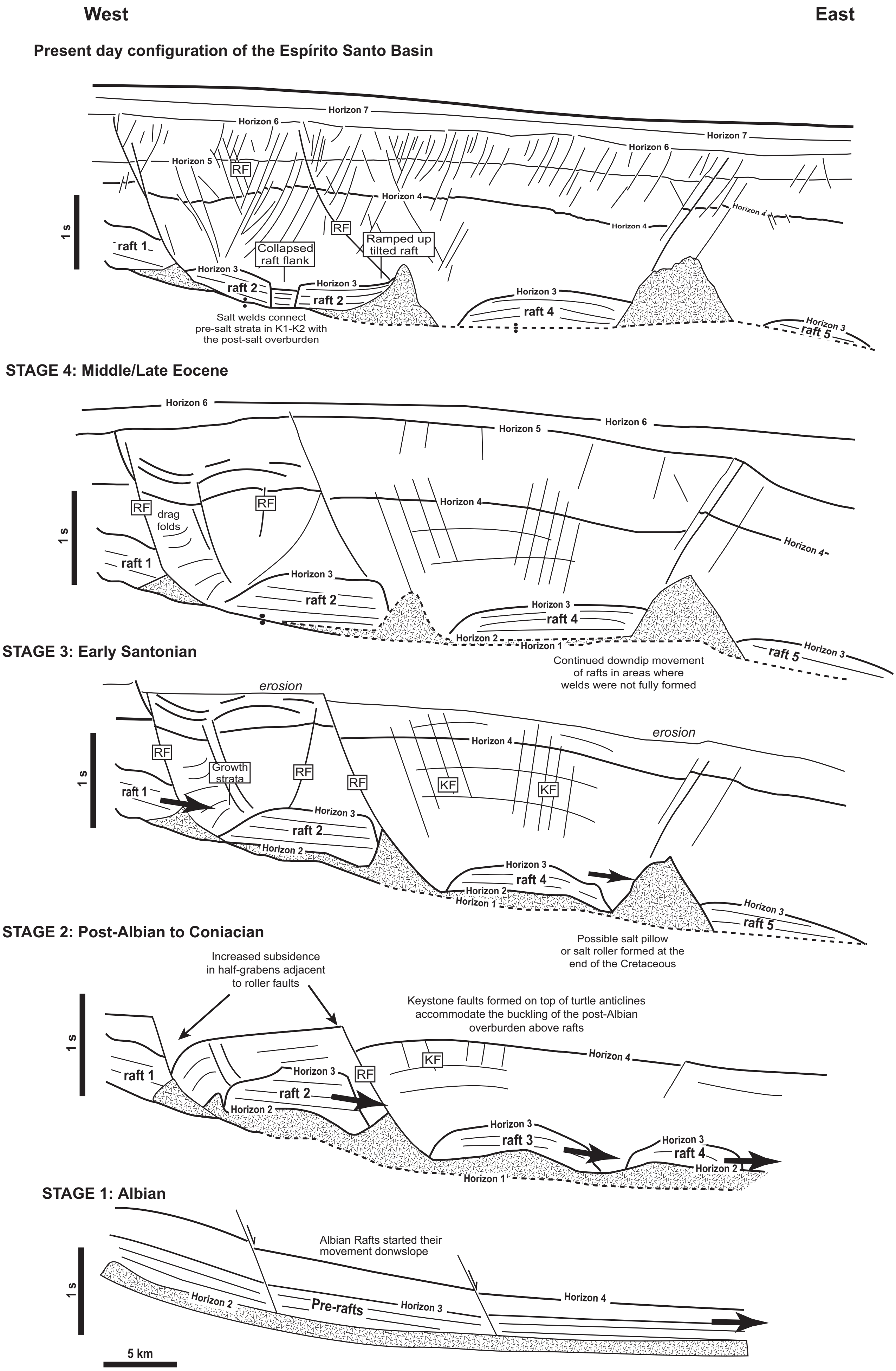
West
East
Present day configuration of the Espírito Santo Basin
Horizon 7
Horizon 6
Horizon 7
Horizon 6
Horizon 5
RF
Horizon 4
Horizon 4
Horizon 4
1 s
raft 1
RF
Collapsed raft flank
Ramped up tilted raft
Horizon 3
raft 2
Horizon 3
raft 2
Horizon 3
raft 4
Horizon 3
raft 5
Salt welds connect pre-salt strata in K1-K2 with the post-salt overburden
STAGE 4: Middle/Late Eocene
Horizon 6
Horizon 5
Horizon 6
RF
drag folds
RF
Horizon 4
Horizon 4
1 s
raft 1
Horizon 3
raft 2
Horizon 3
raft 4
Horizon 2
Horizon 1
raft 5
Horizon 3
STAGE 3: Early Santonian
Continued downdip movement of rafts in areas where welds were not fully formed
erosion
erosion
Horizon 4
RF
Growth strata
RF
RF
KF
KF
1 s
raft 1
Horizon 3
raft 2
Horizon 2
Horizon 3
raft 4
Horizon 2
Horizon 1
Horizon 3
raft 5
STAGE 2: Post-Albian to Coniacian
Possible salt pillow or salt roller formed at the end of the Cretaceous
Increased subsidence in half-grabens adjacent to roller faults
Keystone faults formed on top of turtle anticlines accommodate the buckling of the post-Albian overburden above rafts
1 s
KF
Horizon 4
raft 1
Horizon 3
RF
raft 2
Horizon 2
Horizon 3
raft 3
Horizon 3
raft 4
Horizon 2
Horizon 1
STAGE 1: Albian
Albian Rafts started their movement donwslope
1 s
Horizon 2
Pre-rafts
Horizon 3
Horizon 4
5 km

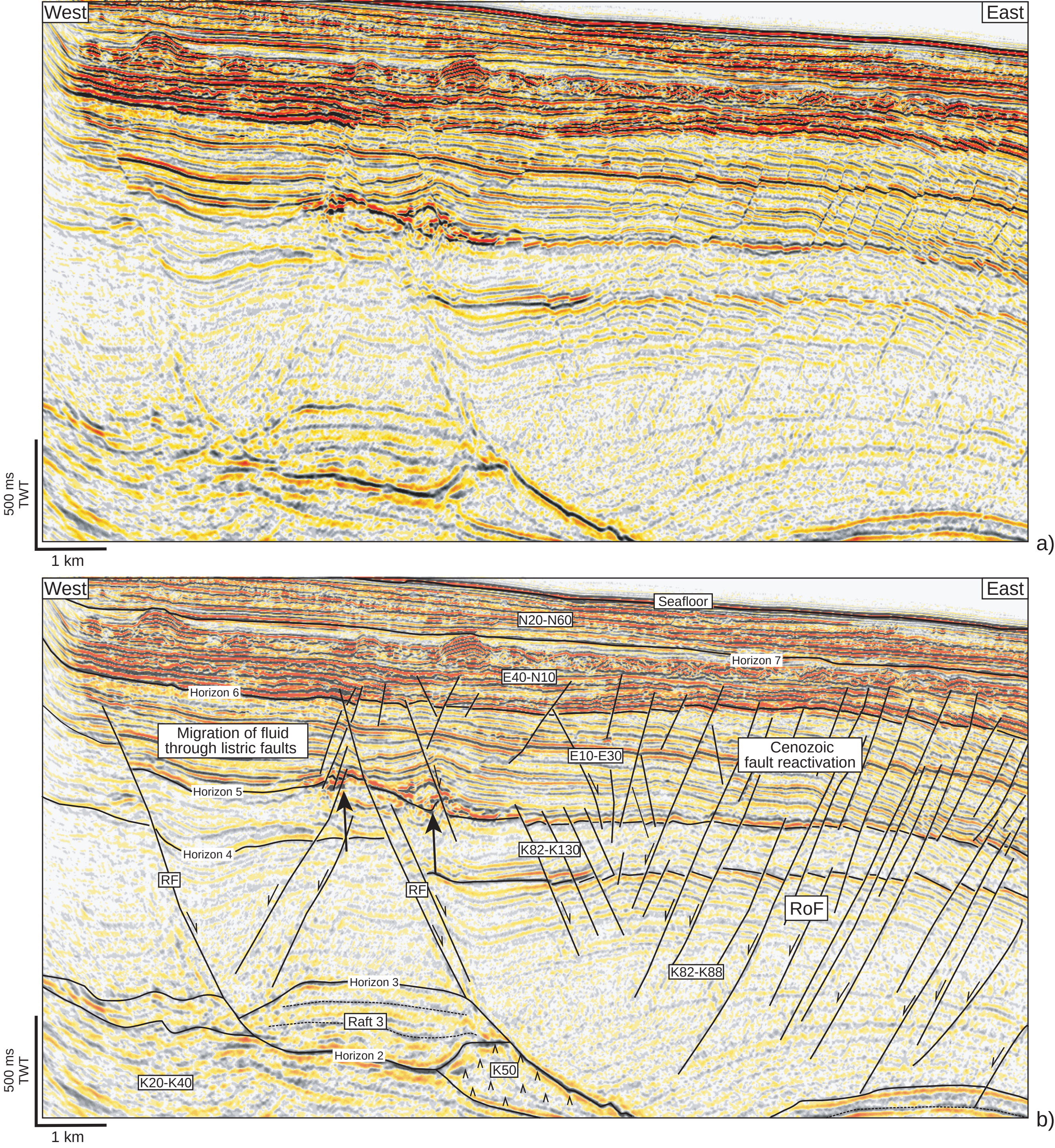
West
East
500 ms TWT
1 km
a)
West
East
Seafloor
N20-N60
Horizon 7
E40-N10
Horizon 6
Migration of fluid through listric faults
E10-E30
Cenozoic fault reactivation
Horizon 5
K82-K130
Horizon 4
RF
RF
RoF
K82-K88
Horizon 3
Raft 3
Horizon 2
K50
K20-K40
500 ms TWT
1 km
b)